GREEN SYNTHESIS AND CHARACTERIZATION OF COPPER OXIDE NANOPARTICLES USING *Hylocereus polyrhizus* PEEL EXTRACT FOR ANTICANCER STUDIES ON COLON (HCC2998) CARCINOMA CELLS

CHEAH QIAN QIAN

BACHELOR OF SCIENCE (HONOURS)

BIOMEDICAL SCIENCE

FACULTY OF SCIENCE

UNIVERSITI TUNKU ABDUL RAHMAN

MAY 2024

GREEN SYNTHESIS AND CHARACTERIZATION OF COPPER OXIDE NANOPARTICLES USING *Hylocereus polyrhizus* PEEL EXTRACT FOR ANTICANCER STUDIES ON COLON (HCC2998) CARCINOMA CELLS

By

CHEAH QIAN QIAN

A project report submitted to the Department of Allied Health Sciences

Faculty of Science

Universiti Tunku Abdul Rahman

in partial of fulfillment of the requirements for the degree of

Bachelor of Science (Honours) Biomedical Science

May 2024

ABSTRACT

GREEN SYNTHESIS AND CHARACTERIZATION OF COPPER OXIDE NANOPARTICLES USING *Hylocereus polyrhizus* PEEL EXTRACT FOR ANTICANCER STUDIES ON COLON (HCC2998) CARCINOMA CELLS

Cheah Qian Qian

The application of metal oxide nanoparticles in cancer treatment is considered a novel invention in the field of biomedicine, replacing traditional radiation and chemotherapy treatments. In this study, an economical and sustainable synthesis of copper oxide nanoparticles (CuO NPs) was implemented via a green approach, using the peel extraction of *Hylocereus polyrhizus* via freeze dried method and copper nitrate trihydrate as the precursor. The synthesized CuO NPs were characterized by analytical equipment such as UV-Visible spectroscopy (UV-Vis), Field Emission Scanning Electron Microscopy (FE-SEM), Energy Dispersive X-ray (EDX), X-ray Diffraction (XRD), and Fourier Transform Infrared Spectroscopy (FTIR). The analysis obtained from UV-Vis spectroscopy presented the wavelength of CuO NPs at 286 nm. A band gap energy of 4.15 eV was determined from the Tauc plot. The SEM analysis displayed 24.9 to 35.4 nm size range for the spherical nanoparticles. The EDX spectrum proved the purity of the *H. polyrhizus*-mediated CuO NPs. The patterns of XRD peaks showed a

monoclinic lattice of CuO NPs, with a crystalline dimension of 23.62 nm. The FTIR spectrum revealed the diverse phytochemical elements found in *H. polyrhizus* extract, which play a crucial role as capping and reducing agents during the synthesis of CuO NPs. The cytotoxic effect of the green-synthesized CuO NPs was tested on the colon carcinoma (HCC2998) cell line via MTT assay. Cell viability was reduced with increasing concentrations of CuO NPs. CuO NPs acted in a dose-dependent mode and showed a high cytotoxic activity towards the colon carcinoma cells, whereas exhibited lesser toxicity towards the Vero cells. This study suggests that *H. polyrhizus*-mediated CuO NPs can be utilized as a promising cytotoxic agent in the biomedical field, because they have the potential to selectively target and kill malignant cells, while sparing normal healthy cells.

ACKNOWLEDGEMENTS

First and foremost, I would like to express my deepest gratitude to my supervisor, Dr. Sinouvassane Djearamane, for his continuous support, patience, and encouragement throughout the journey to completion of this research project. His invaluable advice and feedback gave me the confidence in completing my project. I am really grateful to be guided and supervised by him.

I would like to extend my sincere appreciation to UTAR's Faculty of Science for giving me the opportunity to complete my final year project with the facilities and equipment provided. Moreover, I would like to take this opportunity to thank Ms. Hemaroopini, Mr. Saravanan, Mr. Leong Thung Lim, Mr. Nicholas Ooh Keng Fei, Mr. Seou Chi Kien, and other lab officers for their continuous assistance in handling complex equipment, providing the necessary consumables, chemicals, and chemical glassware throughout the project.

I am deeply indebted to my family for their unconditioned love, encouragement, and understanding. Their constant support has been my pillar of strength, motivating me to strive for excellence.

Last but not least, I am grateful to have my bench mates and friends, who helped me unconditionally by giving me advice and support throughout the FYP journey.

DECLARATION

I hereby declare that the project report is based on my original work except for the quotations and citations which have been dully acknowledged. I also declare that it has not been previously or concurrently submitted for any other degree at UTAR or other institutions.

(CHEAH QIAN QIAN)

APPROVAL SHEET

This final year project report entitled "**GREEN SYNTHESIS AND CHARACTERIZATION OF COPPER OXIDE NANOPARTICLES USING *Hylocereus polyrhizus* PEEL EXTRACT FOR ANTICANCER STUDIES ON COLON (HCC2998) CARCINOMA CELLS**" was prepared by CHEAH QIAN QIAN and submitted as partial fulfilment of the requirements for the degree of Bachelor of Science (Honours) Biomedical Science at Universiti Tunku Abdul Rahman.

Approved by:

(Dr. Sinouvassane Djearamane) Date: 06/06/2024

Supervisor

Department of Allied Health Sciences

Faculty of Science

Universiti Tunku Abdul Rahman

FACULTY OF SCIENCE

UNIVERSITI TUNKU ABDUL RAHMAN

Date: 06/06/2024

PERMISSION SHEET

It is hereby certified that **CHEAH QIAN QIAN** (ID No: **2002040**) has completed this final year project report entitled "GREEN SYNTHESIS AND CHARACTERIZATION OF COPPER OXIDE NANOPARTICLES USING *Hylocereus polyrhizus* PEEL EXTRACT FOR ANTICANCER STUDIES ON COLON (HCC2998) CARCINOMA CELLS" under the supervision of Dr. Sinouvassane Djearamane from the Department of Allied Health Sciences, Faculty of Science.

I hereby give permission to the University to upload the softcopy of my final year project report in PDF format into the UTAR Institutional Repository, which may be made accessible to the UTAR community and public.

Yours truly,

(CHEAH QIAN QIAN)

TABLE OF CONTENTS

		Page
ABSTRACT		**ii**
ACKNOWLEDGEMENTS		**iv**
DECLARATION		**v**
APPROVAL SHEET		**vi**
PERMISSION SHEET		**vii**
TABLE OF CONTENTS		**viii**
LIST OF TABLES		**x**
LIST OF FIGURES		**xi**
LIST OF ABBREVIATIONS		**xiii**
CHAPTER		
1.0	**INTRODUCTION**	**1**
1.1	Research Background	1
1.2	Problem Statement	4
1.3	Research Objectives	5
1.4	Hypothesis	5
1.5	Significance of the Study	6
1.6	Scope of Study	6
2.0	**LITERATURE REVIEW**	**7**
2.1	Green Synthesis of Copper Oxide Nanoparticles	7
2.2	*Hylocereus polyrhizus*	10
2.3	Cancer and Natural Products as Anticancer Agents	13
2.4	Colon Cancer (HCC2998) Cell Line	15
2.5	Vero Cell Line	15
2.6	Cytotoxicity Assay	16
3.0	**MATERIALS AND METHODS**	**21**
3.1	Materials	21
3.1.1	*Hylocereus polyrhizus* Peels	21
3.1.2	Cell Lines	21
3.1.3	Chemical Reagents and Materials	22
3.1.4	Equipment	23
3.2	Methodology	24
3.2.1	Overview of Research Methodology	24
3.3	Green Synthesis of CuO Nanoparticles	25
3.3.1	Preparation of *H. polyrhizus* Peels Extract	25
3.3.2	Green Synthesis of Copper Oxide Nanoparticles	26
3.4	Characterization of CuO Nanoparticles	27
3.4.1	UV-Visible Spectroscopy (UV-Vis)	27
3.4.2	Field Emission Scanning Electron Microscopy (FE-SEM)	27

3.4.3 Energy Dispersive X-ray Spectroscopy (EDX) 27
3.4.4 X-ray Diffraction (XRD) 27
3.4.5 Fourier Transform Infrared Spectroscopy (FT-IR) 28
3.5 Culture and Subculture of Cells 28
3.6 Counting of Cells 29
3.7 MTT Assay 31
3.8 Statistical Analysis 33

4.0 RESULTS 34

4.1 Characterization of the Green-Synthesized CuO NPs 34
4.1.1 UV-Visible Spectroscopy Analysis 34
4.1.2 Field Emission Scanning Electron Microscopy Analysis 36
4.1.3 Energy Dispersive X-ray Analysis 38
4.1.4 X-ray Diffractometry Analysis 39
4.1.5 Fourier Transform Infrared Spectroscopy Analysis 41
4.2 MTT Assay 43
4.2.1 HCC2998 Cells 43
4.2.2 Vero Cells 50

5.0 DISCUSSION 57

5.1 Characterization of the Green-Synthesized CuO NPs 57
5.1.1 Absorbance and Bandgap Energy 57
5.1.2 Surface Morphology 58
5.1.3 Elemental Compositions 59
5.1.4 Crystallite Structure and Size 60
5.1.5 Functional Groups 60
5.2 Cytotoxic Effect of the *H. polyrhizus*-mediated CuO NPs 62
5.3 Limitations of the Study 69
5.4 Future Studies 70

6.0 CONCLUSIONS 71

REFERENCES 72

LIST OF TABLES

Table		Page
2.1	CuO NPs synthesized via plant-mediated methods	9
2.2	Different types of *Hylocereus* species	11
2.3	Taxonomy of *Hylocereus polyrhizus*	11
2.4	Different types of cytotoxicity assays	19
3.1	List of chemical reagents and materials used in this research	22
3.2	List of equipment used during the study	23
4.1	Weight of the elements present in *H. polyrhizus*-mediated CuO NPs	38
4.2	FT-IR analysis on the molecular motion and possible functional groups present in the *H. polyrhizus*-mediated CuO NPs	43
4.3	Percentage of cell viability of HCC2998 cells treated with various concentrations of CuO NPs and cisplatin with 24 hours treatment	45
4.4	Percentage of cell viability of HCC2998 cells treated with various concentrations of CuO NPs and cisplatin with 48 hours treatment	46
4.5	IC_{50} values of *H. polyrhizus*-mediated CuO NPs treatment after 24- and 48-hours against HCC2998 cells	49
4.6	Percentage of cell viability of Vero cells treated with various concentrations of CuO NPs and DMSO with 24 hours treatment	52
4.7	Percentage of cell viability of Vero cells treated with various concentrations of CuO NPs and DMSO with 48 hours treatment	53

LIST OF FIGURES

Figure		Page
1.1	Illustration of the "top-down" and "bottom-up" approaches for the synthesis of nanoparticles	3
2.1	*Hylocereus polyrhizus*	11
2.2	The structure of MTT and formazan product	17
3.1	An overview of the research methodology	24
3.2	Workflow for the preparation of the *H. polyrhizus* peel extract	25
3.3	Workflow for the green synthesis of CuO NPs	26
3.4	Grid lines of one chamber of a haemocytometer and the rule of cell counting	30
3.5	Layout of 96-well plate for MTT assay	32
4.1	UV-Visible absorption spectrum of CuO NPs	35
4.2	Band gap energy for the green-synthesized CuO NPs	35
4.3a	Morphology of the CuO NPs under 20000x magnification	36
4.3b	Morphology of the CuO NPs under 80000x magnification	37
4.4	EDX spectrum of *H. polyrhizus*-mediated CuO NPs	38
4.5	XRD patterns of *H. polyrhizus*-mediated CuO NPs from 10° to 80°	39
4.6	FT-IR spectrum for *H. polyrhizus*-mediated CuO NPs.	42
4.7	Morphology of HCC2998 cells cultured in CGM under 100x magnification	43
4.8	The percentage of cell viability of HCC2998 cells against different concentrations of CuO NPs and cisplatin at 24 hours incubation	45
4.9	The percentage of cell viability of HCC2998 cells against different concentrations of CuO NPs and cisplatin at 48 hours incubation	46

4.10	HCC2998 with various concentrations of CuO NPs after 24 hours under 100x magnification. (A) Negative control, (B) 1.56 µg/mL, (C) 3.13 µg/mL, (D) 6.25 µg/mL, (E) 12.50 µg/mL, (F) 25.00 µg/mL, (G) 50.00 µg/mL, (H) 100.00 µg/mL, (I) Positive control	47
4.11	HCC2998 with various concentrations of CuO NPs after 48 hours under 100x magnification. (A) Negative control, (B) 1.56 µg/mL, (C) 3.13 µg/mL, (D) 6.25 µg/mL, (E) 12.50 µg/mL, (F) 25.00 µg/mL, (G) 50.00 µg/mL, (H) 100.00 µg/mL, (I) Positive control	48
4.12	Morphology of the Vero cells cultured in CGM under 100x magnification	50
4.13	The percentage of cell viability of Vero cells against different concentrations of CuO NPs and DMSO at 24 hours incubation	52
4.14	The percentage of cell viability of Vero cells against different concentrations of CuO NPs and DMSO at 48 hours incubation	53
4.15	Vero cells with various concentrations of CuO NPs after 24 hours under 100x magnification. (A) Negative control, (B) 1.56 µg/mL, (C) 3.13 µg/mL, (D) 6.25 µg/mL, (E) 12.50 µg/mL, (F) 25.00 µg/mL, (G) 50.00 µg/mL, (H) 100.00 µg/mL, (I) Positive control	55
4.16	Vero cells with various concentrations of CuO NPs after 48 hours under 100x magnification. (A) Negative control, (B) 1.56 µg/mL, (C) 3.13 µg/mL, (D) 6.25 µg/mL, (E) 12.50 µg/mL, (F) 25.00 µg/mL, (G) 50.00 µg/mL, (H) 100.00 µg/mL, (I) Positive control	56

LIST OF ABBREVIATIONS

CGM	Complete growth medium
$Cu(NO_3)^2 \cdot 3H_2O$	Copper nitrate trihydrate
CuO NPs	Copper oxide nanoparticles
DMEM	Dulbecco's Modified Eagle Medium
DMSO	Dimethyl sulfoxide
EDTA	Ethylenediaminetetraacetic acid
EDX	Energy Dispersive X-ray Spectroscopy
FE-SEM	Field Emission Scanning Electron Microscopy
FT-IR	Fourier Transform Infrared Spectroscopy
HCC2998	Hamon Cancer Center 2998 (colon cancer cells)
IC_{50}	Half-maximal inhibitory concentration
MTT	3-(4,5-dimethylthiazol-2-yl)-2,5-diphenyltetrazolium bromide
PBS	Phosphate-buffered saline
ROS	Reactive oxygen species
UV-Vis	Ultraviolet-Visible
XRD	X-ray Diffraction

CHAPTER 1

INTRODUCTION

1.1 Research Background

The Greek word ‘nano’, which means remarkably small is used for the measurement of one billionth of a metre (10^{-9} m). Nanoscience studies structures and molecules on the nanoscale, which ranges from 1 to 100 nm, whereas nanotechnology is the discipline associated with technology that uses nanoscience for practical applications, resulting in the development of new nanomaterials and nanosized components (Sim and Wong, 2021). In the 21st century, nanotechnology has emerged as one of the most fascinating novel discoveries by its capacity to apply the theory of nanoscience to real-world settings by monitoring, quantifying, assembling, regulating, and producing matter at the nanoscale. The National Nanotechnology Initiative (NNI) in the United States suggested two settings for nanotechnology. Firstly, the goal of nanotechnology is to manipulate structures at the nanoscale in terms of size and shape. Secondly, given the nature of nanoscale, nanotechnology aims to handle small structures in a way that maximizes their qualities (Bayda, et al., 2020). As a result, in the field of industrial applications and medical devices, like drug delivery systems, imaging probes, and diagnostic biosensors, all of them are now highly dependent on the implementation of the concepts of nanotechnology and nanoscience. Nanotechnology has also brought significant advances to the broad field of biomedicine, especially in cancer therapeutics, due to its enormous capacity to provide novel methods of getting over the challenges imposed by conventional radiation and chemotherapy treatments (Bayda, et al., 2020).

With respect to the high density, strong reactivity, and high surface area-to-volume ratio, nanomaterials provide additional functions in addition to improved selectivity and reactivity (Alhalili, 2023). Metal oxide nanoparticles are renowned for their excellent stability and extensive applicability across various fields, including battery technology, antibacterial research, electronics, photocatalysis, and other areas. However, toxic chemical reagents and solvents, stabilizing agents that are not biodegradable, high temperatures, and labor-intensive processes are all always involved in these approaches, leading to potential toxicity and environmental concerns (Varughese, Kaur and Singh, 2020; Priya, et al., 2023). Therefore, a simple and eco-friendly process for synthesizing nanoparticles is highly sought to address these issues. Due to the natural resources being employed, plant extracts are great sources of material for the easy and ecologically friendly industrial manufacture of metal or metal oxide nanoparticles with regulated sizes and shapes (Priya, et al., 2023). The utilization of green reducing agents like plant-based extracts combined with the accelerated procedure is claimed to be much more budget-friendly, biocompatible, and ecologically friendly from the standpoint of green synthesis. Various components of plant extracts, including fruits, roots, stems, or leaves, have been widely utilized in the production of metal oxide nanoparticles (Koteeswari, et al., 2022). Metal nanoparticles can be synthesized through both “top-down” and “bottom-up” methodologies, as shown in **Figure 1.1**. Generally, the “top-down” method uses various physical or chemical techniques such as mechanical grinding and thermal decomposition to create small metal nanoparticles from bulk metallic components, while “bottom-up” synthesis forms nanoparticles by stacking the metal atoms via chemical or biosynthesis (Bao, et al., 2021).

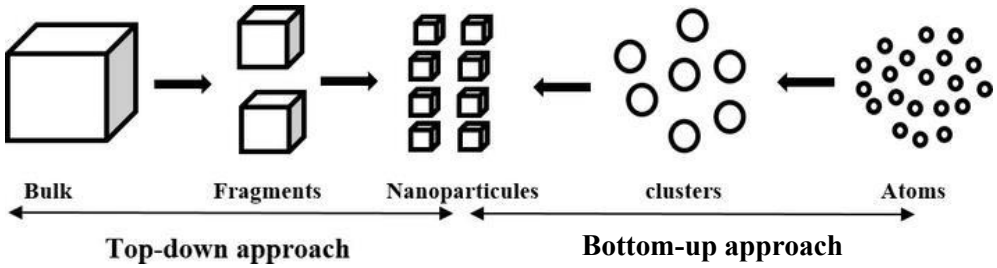

Figure 1.1: Illustration of the "top-down" and "bottom-up" technologies for the formation of nanoparticles (Adapted from Messaoudi and Bendahou, 2020).

Today, metal oxide nanoparticles, such as copper oxide (CuO) have garnered significant interest mainly because of their antimicrobial and biocidal properties, and they possess extensive use across various applications in healthcare sector. According to Tulinska, et al. (2022), CuO NPs have demonstrated their potential in biological and pharmaceutical applications, such as wound healing promoters, drug delivery agents, as well as antibacterial, antifungal, and anticancer agents. Other than biomedical applications, with its distinct optical, electrical, and magnetic characteristics, copper oxide, functioning as a semiconductor metal, has been incorporated into a diverse array of products, including magnetic storage media, semiconductors, infrared filters, sensors, and catalysis.

Cancer is a disorder characterized by the uncontrolled proliferation of certain body cells, which invade surrounding tissues. Human cells normally grow and multiply through regulated division of cells to produce newly developed cells whenever needed by the body. Damaged or aged cells are typically programmed to undergo cell death and be replenished by new, healthy cells. Cancerous cells, however, disrupt the normal biological process, resulting in the indefinite growth and proliferation of the abnormal or damaged cells (National Cancer Institute, 2021). The World Health Organization (2024) has projected a significant increase in cancer cases globally, with over 35 million new cases anticipated by 2050. This represents a 77% rise from the estimated 20 million cases reported in 2022. According to Gleneagles Hospitals (2022) and Wong, et al. (2022), lung cancer, colon cancer, breast cancer, liver cancer, and nasopharyngeal cancer are among the top five most prevalent malignancies among the Malaysian population.

1.2 Problem Statement

The upward trend and mortality rate of cancer have become a global public health concern. Treating cancer has also been a highly complex process. Several types of traditional cancer treatment are available nowadays, including radiation therapy, chemotherapy, and surgery (Debela, et al., 2021). However, the main concerns and significant drawbacks of traditional therapy are the high cost of cancer drugs and treatments, and the adverse side effects and toxicities of synthetic cancer medications. Therefore, the emergence of nanoparticles as one of the new cancer treatments creates a new alternative that is more financially affordable and more specific to the target cells.

1.3 Research Objectives

The research objectives for this project are:

1. To green synthesize the CuO NPs by using *Hylocereus polyrhizus* peel extract as capping and reducing agent.

2. To characterize the green-synthesized CuO NPs using various analytical instruments, including UV-Visible spectroscopy (UV-Vis), Field Emission Scanning Electron Microscopy (FE-SEM), Energy Dispersive X-ray Spectroscopy (EDX), X-ray Diffraction (XRD), and Fourier Transform Infrared Spectroscopy (FTIR).

3. To evaluate the cytotoxic effect of the CuO NPs against colon carcinoma (HCC2998) cells using MTT assay.

1.4 Hypothesis

The hypotheses of this study are:

1. Can the green-synthesized CuO NPs be efficiently synthesized using *Hylocereus polyrhizus* peel extract as the capping and reducing agent?

2. Does CuO NPs show selective cytotoxicity effect on the colon carcinoma cells?

1.5 Significance of the Study

There is very limited research that focuses on the anticancer effect of CuO NPs. This statement would likely prompt public and researcher inquiries regarding the potential cytotoxic effects of CuO NPs on cancer cells. In addition, currently there is no study regarding the anticancer activity of CuO NPs on the colon carcinoma (HCC2998) cell line. This leads to the significance of the present study to evaluate whether CuO NPs are effective as an alternative cancer agent to treat colon cancer cells in the future.

1.6 Scope of Study

In this study, CuO NPs were produced via the green synthesis approach, without the addition of sodium hydroxide to adjust the pH while green synthesizing the CuO NPs. Sodium hydroxide and *Hylocereus polyrhizus* can both function as capping and reducing agents in this research study. However, given that the study's title focused on the green-synthesis method, fruit peel extract mostly plays the role of a capping and reducing agent rather than chemical synthesis. Besides, the green-synthesized CuO NPs were further characterized via several analytical instruments in order to validate the various characteristics of a nanoparticle. Finally, MTT assay was performed to assess the cytotoxic potential of CuO NPs against both normal and malignant cells.

CHAPTER 2

LITERATURE REVIEW

2.1 Green Synthesis of Copper Oxide Nanoparticles

Researchers place particular emphasis on copper oxide nanoparticles due to their wide-ranging applications in fields such as photocatalysis, superconductivity, biosensors, and biomedicine. Consequently, the adoption of green synthesis techniques for CuO NPs, which are green and ecologically sustainable has gained significant traction as a replacement for traditional approaches to synthesis (Badri, et al., 2021). Due to the fact that in green synthesis, instead of chemicals, plant-mediated products are more likely to perform the function as reducing agents. Various metabolites and functional groups present in the biological products play important roles in reducing, chelating, stabilizing, and synthesizing nanoparticles. Thus, it is valuable in lessening the toxic effects of chemicals in the environment and is cost-effective (Ramasubbu, et al., 2023).

Natural extracts of plants, microbial organisms, and other biotic products have been used for the fabrication of CuO NPs via an eco-friendly method (Waris, et al., 2021). A green technique has the advantage of reducing the use of toxic materials, costly instruments, and meticulous oversight of the reduction process while also being safer and harmless to the environment (Badri, et al., 2021; Ramasubbu, et al., 2023). According to Waris, et al. (2021), CuO NPs produced via environmentally sustainable methods are recognized for their safety, eco-friendliness, economic viability, and stability.

According to Waris, et al. (2021), copper (Cu) is a vital micronutrient necessary for the health and well-being of humans, animals, and plants. Humans require only a small quantity of copper in the bodies. The daily copper intake is approximately 2 to 4 mg, and it has to be taken from sources in the diet such as food or beverages. Besides, copper plays an important part in the human body. It serves as a regulator of cell signalling pathways, acts as a cofactor for several enzymes engaged in the synthesis of neuropeptides, and contributes to the capability of human immune cells responsible for the elimination of pathogens. Meanwhile, copper is a necessity in plants for different types of biochemical and physiological mechanisms. It is also among the essential trace elements required for the development and growth of plants. For example, serving as the enzyme's cofactor, it helps to ensure the proper functioning of key proteins and enzymes like plastocyanin, amino oxidase, and cytochrome c oxidase (Waris, et al., 2021).

As reported by several research studies, plant-derived extracts are a preferable resource for nanoparticle production as compared to microorganisms (Kumar, et al., 2015; Ijaz, et al., 2017; Yugandhar, et al., 2017). This is because the tedious procedure of isolating microbes can be excluded, and microbial toxicity can be eliminated. In addition, as presented in **Table 2.1**, phenols, flavonoids, terpenoids, and tannins are among the metabolites found in plant extracts. They serve as both reducing and capping agents, facilitating the reduction of metallic ions into their respective nanoparticles. Moreover, the plant extract will produce electrons, and copper salts will be reduced. Subsequently, the phytochemicals interact with the copper ions, inducing reduction and ultimately resulting in the formation of CuO NPs (Waris, et al., 2021).

Table 2.1: CuO NPs synthesized via plant-mediated methods.

Plant Name	Part Used	Phytochemical Components	Size and Shape	References
Punica granatum	Peel extract	Amides, alcohols, phenols, and other molecules containing carbonyl group	40 nm, spherical shape	Ghidan, Al-Antary and Awwad, 2016
Musa acuminata	Peel extract	Flavonoids, phenolics, saponins, tannins, and carotenoids	60 nm, spherical shape	Aminuzzaman, Kei and Liang, 2017; Mathew and Negi, 2017
Erzincan cimin	Fruit extract	Phenolic acids, flavonoids, anthocyanins, and proanthocyanidins	25-50 nm, spherical shape	Gultekin, et al., 2017
Phoenix dactylifera	Fruit extract	Phenolic acids, tannins, and flavonoids	78 nm, spherical shape	Mohamed, 2020
Ziziphus mauritiana	Plant extract	Tannins, coumarins, saponins, flavonoids, and glycosides	20-45 nm, spherical shape	Pansambal, et al., 2017
Aloe vera	Leaf extract	Alkanes, alkenes, and other molecules containing hydroxyl group	20 nm, spherical shape	Kumar, et al., 2015
Malva sylvestris	Leaf extract	Alcohol, phenols, flavonoids, amide	14 nm, spherical shape	Awwad, Albiss and Salem, 2015

2.2 *Hylocereus polyrhizus*

The red-fleshed pitaya or dragon fruit, namely *Hylocereus polyrhizus*, is a type of tropical fruit that originated in Mexico, but it is currently grown on a large scale all over the world, including Vietnam, Israel, Taiwan, Southern China, and most recently in Australia, Thailand, America, as well as Malaysia (Miranda-Castro, 2016). It has gained attention from all around the world because of its unique flavor, vibrant color, and appealing appearance, in addition to its many advantages for personal health (Abirami, et al., 2021). As shown in **Table 2.2**, the scientific name of dragon fruit is assigned based on its color of peel and pulp. As shown in **Figure 2.1**, the peel and flesh of *H. polyrhizus* are purple red in color, given its well-known strong antioxidant capacity. According to Wybraniec, et al. (2007), the red color of *H. polyrhizus* is due to the betacyanin component, which is a type of water-soluble pigment. The yellow betaxanthins and reddish violet betacyanins are components of the betalain pigments, which are the characteristics of plants in the *Caryophyllales* order (Phebe, et al., 2009). The taxonomy of *H. polyrhizus* is shown in **Table 2.3**. Moreover, *H. polyrhizus* is rich in essential nutrients such as minerals, vitamins, carbohydrates, dietary fibers, and antioxidants. For instance, phenols and flavonoids are examples of antioxidant constituents found in *H. polyrhizus*, with their function being to protect against chronic diseases and cancers caused by oxidative stress (Abirami, et al., 2021). According to Mahmud, et al. (2023), many countries have plenty of dragon fruit peels accessible as agricultural waste, including Indonesia, which produces about 150,000 tonnes of dragon fruit annually.

Table 2.2: Different types of *Hylocereus* species.

Name	**Characteristics**
Hylocereus polyrhizus	Red peel with red pulp
Hylocereus undatus	Red peel with white pulp
Hylocereus megalanthus	Yellow peel with white pulp

Figure 2.1: *Hylocereus polyrhizus* (Adapted from Saneto, 2012).

Table 2.3: Taxonomy of *Hylocereus polyrhizus* (Global Biodiversity Information Facility, 2023).

Taxonomy (Scientific Classification)	
Kingdom	Plantae
Phylum	Tracheophyta
Class	Magnoliopsida
Order	Caryophyllales
Family	Cactaceae
Genus	*Hylocereus*
Species	*Hylocereus polyrhizus*

Dragon fruit, as a functional food, can be used to make wine, juice, spreads, pastries, or consumed raw. Sometimes, the flowers are made into tea or consumed as a vegetable (WebMD, 2024). In terms of its applications and medicinal uses, dragon fruit serves as antioxidant, anti-inflammatory, anti-diabetic, antimicrobial, and anticancer agents for the treatment of various illnesses. Owing to these advantageous properties that are greatly beneficial to individuals, the consumption of dragon fruit has surged across several global locations. However, the peels, which are inedible, will be discarded as biowaste. In addition to having numerous technological uses in the food and pharmaceutical industries, dragon fruit also provides new opportunities for the development of multi-targeting medications for the prevention and treatment of various illnesses. Studies have demonstrated that the presence of bioactive components in *H. polyrhizus*, which include potassium, betacyanin, vitamins, p-coumaric acid, and many more, may be useful in dealing with several conditions, including diabetes, cardiovascular diseases, and cancer (Nishikito, et al., 2023).

The outside parts of dragon fruit that are thrown away frequently as organic waste cause major issues with the disposal of solid trash. Therefore, the peels of dragon fruit have become commonly employed in industries across a range of sectors to turn the peel waste into something valuable in order to raise its economic value. As reported by Veerakumar, et al. (2023), *H. costaricensis* peels have been used as an alternative precursor for the production of biomass-derived activated carbon. Other than that, Muhammad, et al. (2020) have conducted their research study on converting dragon fruit peel into consumable pectin to reduce waste generated from the consumption of dragon fruit. In the food sector,

residual peels of dragon fruit have been used to produce betalains and pectin, which can be served as alternative food additive sources (Tran, et al., 2022).

2.3 Cancer and Natural Products as Anticancer Agents

Cancer occurs when cells undergo uncontrolled growth and proliferation, with the ability to invade and damage healthy tissues in the body. When the proliferation of cells is not well-regulated, clusters of cells, which are known as tumors, will form. Malignant (cancerous) tumors can differ from benign (non-cancerous) tumors. Generally, the growth rate of benign tumors is slow, and they do not metastasize. In contrast, cancerous tumors have the ability to spread quickly throughout the body, infiltrate, and kill the neighbouring normal tissues (The University of Kansas Cancer Center, 2024). Cancers have been on the rise because of the significant lifestyle changes brought about by modern living in this era of modernization. It ranks as the second-leading cause of death globally. The hallmarks of cancer tend to involve seven biological traits attained during the multistep evolution of lesions, which are permitting unlimited replication, maintaining proliferative signaling, resisting growth inhibitory signals, evading programmed cell death (apoptosis), activating invasion and metastasis, transforming energy metabolism, and stimulating angiogenesis (Hanahan and Weinberg, 2011). Mutations in cellular DNA serve as the fundamental cause of cancer. DNA comprises of various genes, each containing commands that regulate cell growth and division. Malignant cells can develop from signals that contain errors, which inhibit them from functioning normally (Mayo Clinic, 2022).

According to Ferlay, et al. (2024), the most prevalent forms of cancer incidences in Malaysia for both genders across all ages are breast (16.2%), colorectum (13.8%), lung (10.7%), liver (4.6%), and prostate (4.6%) cancers. In particular, lung (16.9%), colorectum (15.6%), and prostate (9.5%) cancers are the top three leading cancers in men. On the other hand, the top three most prominent cancers in females included breast (31.3%), colorectum (12.2%), and cervix uteri (7.1%) cancers.

With regard to the high fatality rate of cancer worldwide, extensive research has been undertaken to uncover natural anti-tumor drugs that combat cancer cells. There is still an enormous demand for less hazardous and addictive medications, even with the availability of numerous anticancer drugs and therapies today. Based on the diverse range of metal or metal oxide nanoparticles developed through green methods by other researchers, it reveals that nanoparticles hold substantial potential for clinical application in the treatment of cancer in the future.

As reported by Divakaran, et al. (2019), dragon fruit was utilized to synthesize Au NPs, as well as to determine its anticancer properties. The findings highlighted that the nanoparticles were effective in anticancer activity, with an IC_{50} value of 25 µg/mL against the colon cancer (HCT-116) cell line. Another Ag NPs derived from *Hylocereus undatus* by Shyamalagowri, et al. (2022) also proved its anticancer property with an IC_{50} value of 37.98 µg/mL when tested on HepG2 (liver) cancerous cells. Apart from that, Rajagopal, et al. (2021) and Gnanavel, et al. (2017) applied *Wrightia tinctoria* extract and *Ormocarpum*

cochinchinense leaf extract, respectively, to green synthesize their Cu and CuO NPs. The breast cancer (MCF-7) cells and Vero cells with the treatment of Wt-Cu NPs showed IC_{50} values of 119.23 µg/mL and 898.75 µg/mL, respectively. Meanwhile, CuO NPs derived from *O. cochinchinense* leaf extract showed potent cytotoxic effect on colon cancer (HCT-116) cell line, displaying an IC_{50} value of 40 µg/mL. In summary, the aforementioned findings implied that the green-synthesized nanoparticles were non-cytotoxic to normal cells but had a moderately cytotoxic effect on cancer cell lines.

2.4 Colon Cancer (HCC2998) Cell Line

HCC2998 is a type of cancer cell line originated from *Homo sapiens* with the disease of colon adenocarcinoma. HCC2998 are adherent cells with an epithelial-like structure. When cultured HCC2998 cells *in vitro*, these cells will attach to the inner surface of the tissue culture flask and form a monolayer. HCC2998 cells have a doubling time of 31.5 to 44.4 hours (Bazzocco, et al., 2015; National Cancer Institute, 2015).

2.5 Vero Cell Line

In 1962, kidney tissue from a normal, healthy adult African green monkey, named as *Cercopithecus aethiops*, was used to establish the Vero cell line. Many potential applications exist for the cell line, such as the detection of verotoxins, efficacy testing, and 3D cell culture (American Type Culture Collection, 2020).

Vero cell line is an example of an anchorage-dependent (adherent) cell line. It exhibits an epithelial-like shape and tends to form monolayers. These cells typically exhibit an average measurement of around 17 μm and display a rounded to elongated morphology when observing them under an inverted microscope (Cytion, 2024). The doubling time for Vero cells is approximately 24 hours (Ammerman, Beier-Sexton and Azad, 2009).

2.6 Cytotoxicity Assay

MTT (3-[4,5-dimethylthiazol-2-yl]-2,5 diphenyl tetrazolium bromide) assay is the most appropriate cytotoxicity test to assess cell viability and cytotoxicity in anticancer studies among the various varieties of assays, as tabulated in **Table 2.4**. Firstly, MTT test is a popular option in laboratories due to its affordability and ease of use. MTT assay can be completed within five to six hours, with the simple procedures of introducing MTT reagent to cell cultures, incubation, solubilizing the formazan crystals produced by metabolically active cells, and measuring the absorbance by using a microplate reader. MTT assay yields quantitative data on the proliferation and viability of cells. The quantity of formazan produced correlates directly with the number of viable cells present in the culture (Riss, 2024). This makes it possible for researchers to precisely measure the cytotoxic effect on cancer cells of various compounds or treatments. Besides, the high sensitivity of MTT assay enables researchers to detect minute alterations in cell viability, which makes it appropriate for evaluating the effectiveness of possible anticancer drugs or treatments. Given its high sensitivity, researchers can also detect substances at comparatively low concentrations that cause cell death (Tonder, Joubert and Cromarty, 2015).

According to Drug Discovery News (2023), MTT assay is flexible across different cancer models, making it an attractive option for anticancer research.

The MTT assay is extensively recognized as the gold standard of high-throughput cytotoxicity assays (Tonder, Joubert and Cromarty, 2015). MTT test measures mitochondrial activity through the process in which viable cells convert MTT into formazan crystals (**Figure 2.2**), which are the purple-colored product with an absorbance wavelength maximum at 570 nm. In contrast, when cells are not viable, they cease their metabolic activity and are incapable of converting MTT, leading to no observable color change (AAT Bioquest, 2022). This assay is commonly employed to evaluate the *in vitro* cytotoxic effect of drugs on numerous cell lines. The number of viable cells determines the overall mitochondrial activity (Meerloo, Kaspers and Cloos, 2011).

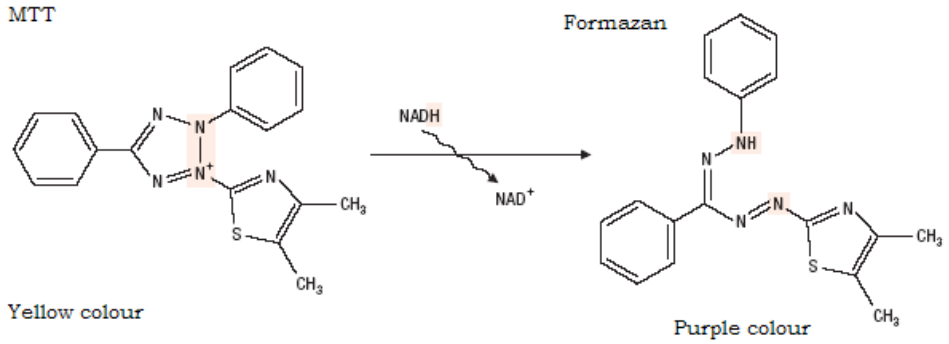

Figure 2.2: The structures of MTT and formazan product (Adapted from Desai, et al., 2011).

As presented in **Figure 2.2**, the MTT reagent is a salt of mono-tetrazolium. The structure of MTT illustrates four nitrogen atoms in a quaternary tetrazole ring core that is positively charged, encircled by three aromatic rings, which comprise two phenyl groups, and another thiazolyl ring (Desai, et al., 2011). Upon reduction of MTT, the core of the tetrazole ring undergoes disruption, resulting in the formation of a purple molecule that is insoluble in nature. Due to its positive ionic state and lipophilic nature, MTT can permeate through both the cell membrane and the inner mitochondrial membrane of living cells. MTT can be reduced intracellularly by the aid of oxidoreductase, dehydrogenase enzymes, and NAD(P)H (electron donors) at several stages of the glycolytic processes. As a result, MTT will be converted to insoluble formazan by cells with active metabolism. Usually, water-insoluble formazan crystals are dissolved using a solvent. For instance, dimethyl sulfoxide (DMSO) will be added prior to absorbance measurement (Ghasemi, et al., 2021).

Table 2.4: Different types of cytotoxicity assays (Toxicology MSDT, 2022).

Assay	**Principle**
DNA fragmentation / Ladder assay	Agarose gel electrophoresis separates fragmented DNA from cells generated by chemicals or medications, which is then visualized as a "ladder" using ethidium bromide staining. The cell death will be assessed.
Comet assay	The amount of damaged DNA is represented as a comet tail moment using micro gel electrophoresis.
Necrosis assay	Cells that showed positive staining in flow cytometry analysis for both FITC Annexin V and PI are transitioning from the apoptotic stage to the necrotic stage, while cells that do not exhibit positive stain for FITC Annexin V or PI are not exhibiting either necrosis or apoptosis.
Enzyme assay	A color change will be spotted upon reactions with a specific probe that signals lactate dehydrogenase passage, which occurs when cell membrane integrity is disrupted by cytotoxic substances.
Proteomics assay	The effect of toxicants in cellular toxicity signaling system will be assessed by detecting the expression of a specific protein, known as biomarker.
Expression array assay	The fluorescent intensity of different genes that are altered by cellular toxicants are evaluated via a chip-based microarray.

After an in-depth literature review, the potential of nanoparticles and *H. polyrhizus* in cancer treatment has been identified. So, in this study, *H. polyrhizus* was chosen as an alternative source of capping and reducing substances in green synthesizing the CuO NPs. The equipment available in the laboratory, such as UV-Visible spectroscopy (UV-Vis), Field Emission Scanning Electron Microscopy (FE-SEM), Energy Dispersive X-ray (EDX), X-ray Diffractometer (XRD), and Fourier Transform Infrared Spectroscopy (FTIR) were applied to characterize and identify the green-synthesized CuO NPs. The cytotoxic effect of CuO NPs were investigated on colon cancer (HCC2998) and Vero cell lines to determine the anticancer potential of the synthesized CuO NPs.

CHAPTER 3

MATERIALS AND METHODS

3.1 Materials

3.1.1 *Hylocereus polyrhizus* Peels

H. polyrhizus (dragon fruits) were purchased from a hypermarket named Lotus's, located in Kampar, Perak.

3.1.2 Cell Lines

CCL-81, also known as the Vero cell (adult African green monkey kidney cell line) and the HCC2998 (human colon carcinoma cell line) were obtained from the Faculty of Science, UTAR, Kampar campus.

3.1.3 Chemical Reagents and Materials

Table 3.1 indicates all the chemical reagents and materials used during the study.

Table 3.1: List of chemical reagents and materials used in this study.

Chemical reagents / Materials	**Source, Country**
0.25% Trypsin-EDTA	GE Healthcare, United States
0.4% Trypan blue dye	Sigma-Aldrich, United States
95% Ethyl acetate (Industrial grade)	Chemical Solutions, Malaysia
96-well plate	Techno Plastic, Switzerland
Basic DMEM powder	Sigma-Aldrich, United States
Cisplatin	EMD Chemicals, Inc. San Diego
Copper nitrate trihydrate	HmbG, Germany
Dimethyl sulfoxide (DMSO)	Fisher Scientific, United Kingdom
Fetal bovine serum	Sigma-Aldrich, United States
Phosphate buffered saline tablet	Oxoid Limited, United Kingdom
Sodium hydrogen carbonate	SYSTERM, Malaysia
Thiazolyl blue tetrazolium bromide, 98%	Merck, Germany

3.1.4 Equipment

Table 3.2 shows all the equipment that were utilized during the study.

Table 3.2: List of equipment used during the study.

Equipment	**Manufacturer / Brand**
5% carbon dioxide (CO_2) incubator	BINDER, Germany
Autoclave	Hirayama, Japan
Centrifuge	Heraeus, Germany
Electronic balance	RGS Corporation Sdn. Bhd., Malaysia
Freezer (-20 °C)	Pensonic, Malaysia
Hemocytometer	Hecht-Assistant, Germany
Inverted phase contrast microscope	Nikon, Japan
Laminar flow cabinet	Esco Micro (M) Sdn. Bhd., Malaysia
Microplate reader	BMG Labtech, Germany
Plant oven / incubator	Memmert, Germany
Refrigerator (4 °C)	Samemax, Malaysia
Scanvac CoolSafe 4 L freeze dryer	LaboGene, Denmark
Sonicator	Elma Schmidbauer GmbH, Germany
Ultra-low freezer (-80 °C)	Eppendorf Asia Pacific, Malaysia
Vortex	PLT Scientific, Malaysia
Water bath	Memmert, Germany

3.2 Methodology

3.2.1 Overview of Research Methodology

Figure 3.1 depicts the simplified workflow of the study. The *H. polyrhizus* peels extract was prepared by the freeze-dried alternative. The synthesized nanoparticles were characterized prior to proceeding to the cytotoxicity testing for HCC2998 colon carcinoma via the MTT assay.

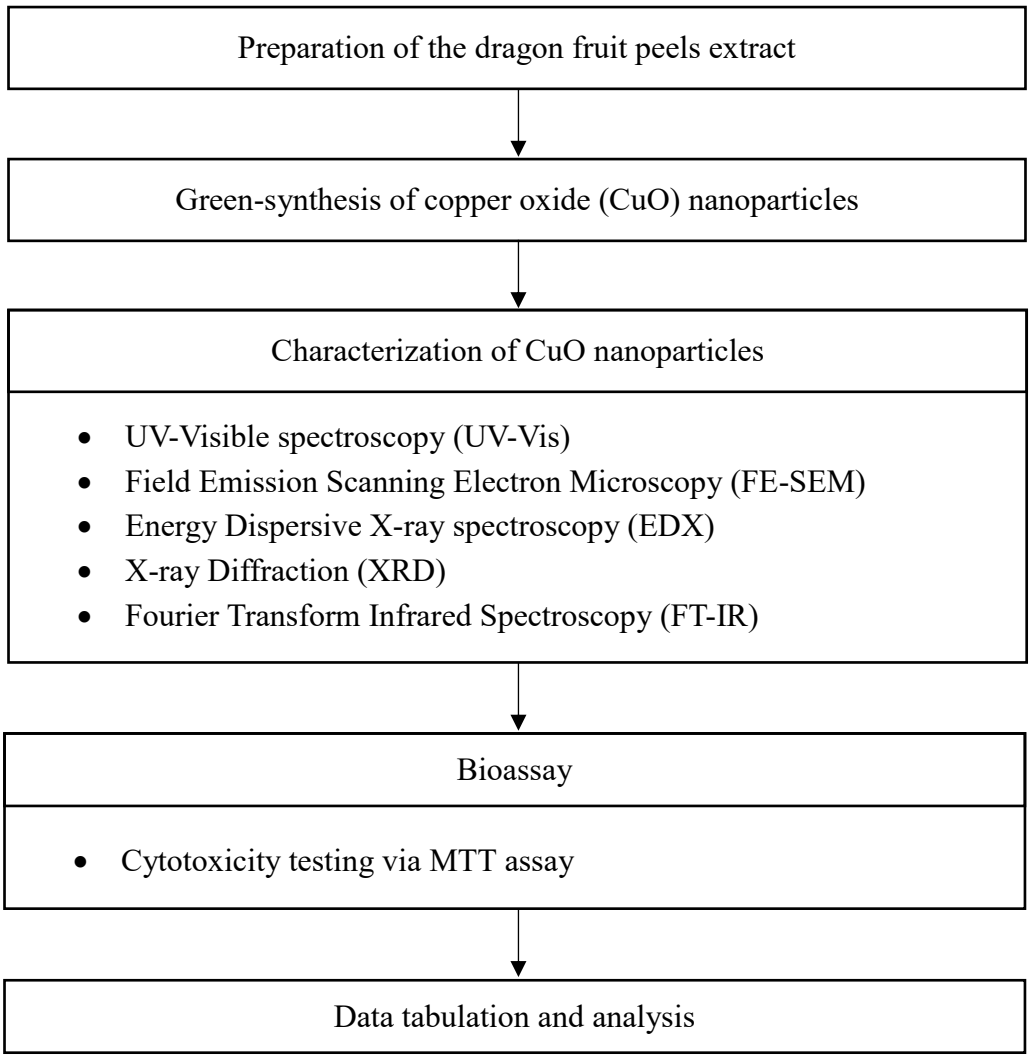

Figure 3.1: An overview of the research methodology.

3.3 Green Synthesis of CuO Nanoparticles

3.3.1 Preparation of *H. polyrhizus* Peels Extract

Figure 3.2 shows the overall workflow for the preparation of *H. polyrhizus* peels extract. The peels were peeled from the fruits and cut into smaller pieces, washed with distilled water, and patted dry with tissue. The peels were incubated in an oven at 60 °C for one day, until all the peels became completely dry and crunchy. The dried peels were then blended into powder form. Approximately 2 L of distilled water were added to 25 g of *H. polyrhizus* powder to form a mixture. The mixture was purified by Whatman filter paper 1 and aliquoted into 50 mL centrifuge tubes for centrifugation. The supernatant was poured into the round-bottomed flasks and left for overnight freezing at a temperature of -20 °C. The frozen samples were subjected to freeze-drying for about a week. Pinkish-red sticky crude extract was observed on the walls of the round-bottomed flasks. The crude extract was scraped off the wall and stored in an airtight Schott bottle.

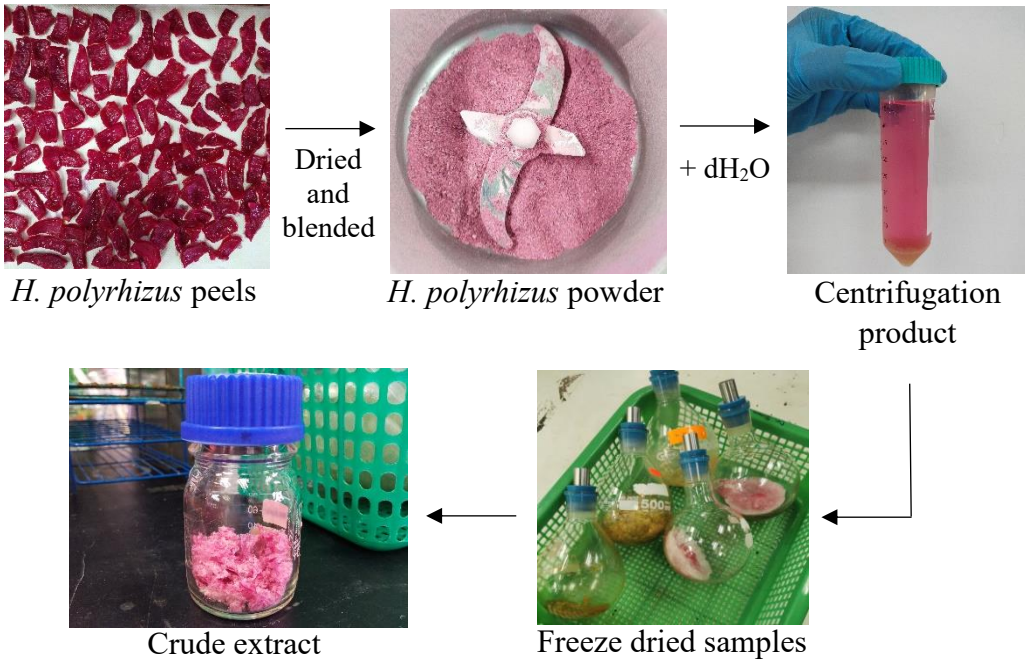

Figure 3.2: Workflow for the preparation of the *H. polyrhizus* peels extract.

3.3.2 Green Synthesis of Copper Oxide Nanoparticles

Figure 3.3 shows the workflow for the green synthesis of CuO NPs. One gram of crude extract was mixed well with 50 mL of distilled water. About 3 g of $Cu(NO_3)^2 \cdot 3H_2O$ was weighed and added to the extract with continuous swirling on a hotplate stirrer at a temperature between 70 °C and 80 °C until saturated. A dark green paste product was formed, and it was transferred into a crucible. The dark green paste was calcinated by the Furnace large Nabertherm at 400 °C for 2 hours (Okpara, et al., 2021). After the process of calcination, black-colored CuO NPs were obtained in the crucible. The CuO NPs were kept in a tightly closed microcentrifuge tube and stored at room temperature until further use.

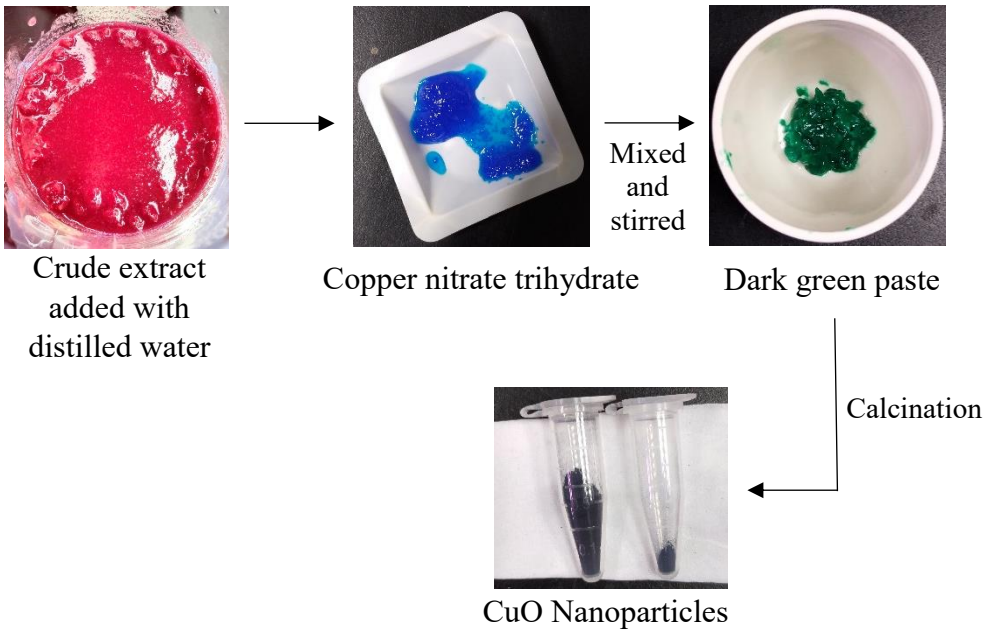

Figure 3.3: Workflow for the green synthesis of CuO NPs.

3.4 Characterization of CuO Nanoparticles

3.4.1 UV-Visible Spectroscopy (UV-Vis)

The green-synthesized CuO NPs from the reduction of the copper ions from the copper nitrate trihydrate precursor were mixed with deionized water, and the mixture was sonicated to form colloid structure before being analyzed by the UV-Visible spectrophotometer (Thermo Fisher Scientific G 10S UV-Vis, United States) at room temperature with a wavelength between 200 nm and 800 nm (Tabrez, et al., 2022; Nzilu, et al., 2023).

3.4.2 Field-Emission Scanning Electron Microscopy (FE-SEM)

The surface structure of the CuO NPs was confirmed by the FE-SEM analysis (JOEL JSM 6710F, Japan).

3.4.3 Energy Dispersive X-ray Spectroscopy (EDX)

The composition of elements of the CuO NPs was detected via electron dispersive X-ray spectroscopy (Oxfords Instrument X-max Energy Dispersive Diffractometer).

3.4.4 X-ray Diffraction (XRD)

The green-synthesized CuO NPs were ensured to be completely dried before characterization by the X-ray diffractometer (Shimadzu XRD 6000, Japan) using the Cu-Kα radiation in the 2θ range of 30° to 70° at a temperature of 25 °C and a voltage of 40 kV and 20 mA current (Nzilu, et al., 2023).

3.4.5 Fourier Transform Infrared Spectroscopy (FT-IR)

The *H. polyrhizus*-mediated CuO NPs were analyzed by FT-IR spectroscopy (Perkin Elmer Spectrum RX-1 FT-IR Spectrometer, USA) to identify the functional groups discovered in the CuO NPs. The CuO NPs were mixed with the KBr in a ratio of 1:10 to form the pellet. The analysis was observed in the scan range of 4000 to 400 cm^{-1} with a resolution of 4 cm^{-1} (Tabrez, et al., 2022).

3.5 Culture and Subculture of Cells

Vero and HCC2998 cell lines were quickly thawed in a water bath (37 °C) for one minute. By using a serological pipette, 4 mL of the pre-warmed complete growth medium (CGM) was added into a new 25 cm^2 tissue culture flask, followed by 1 mL of the thawed cells. The cells were then examined under an inverted microscope and incubated at 37 °C, 5% CO_2 incubator. The cells were observed daily to check for signs of deterioration and contamination.

Subculture of the cells was conducted once the cells had reached a confluency of around 80%. The old media was removed, and 5 mL of phosphate-buffered saline (PBS) was added to rinse the cells twice. The flask was filled with 3 mL of 0.25% trypsin-EDTA solution and incubated for around 15 minutes in the incubator. After the incubation period, the cells were checked under an inverted microscope to confirm the successful detachment of the cells. Then, 3 mL of CGM was pipetted into the flask to deactivate the trypsinization process. The content was carefully poured into a 15 mL centrifuge tube and centrifuged for 10 minutes at 25 °C at 1000 rpm. The supernatant was discarded, and 2 mL of CGM was added to the pellet and resuspended. A new culture flask was prepared

by first adding 4 mL of CGM and subsequently 1 mL of cells. The flasks were incubated in the 5% CO_2 incubator at an average temperature of 37 °C.

3.6 Counting of Cells

Subculture was carried out once the cells had reached confluency of 80%. Approximately 100 µL of the suspension of cells and 100 µL of 0.4% trypan blue were mixed at a 1:1 dilution, into a microcentrifuge tube. The mixture was left to incubate at room temperature for a duration of 3 to 5 minutes. The mixture was then resuspended again to prevent sedimentation and clumping of the cells before loading 10 µL of the mixture into the chambers of a clean hemocytometer. The hemocytometer flooded with cells was viewed under an inverted microscope with a magnification of 100x. Under the microscope, the viable cells were unstained, whereas the dead cells were stained blue. The total number of living cells and dead cells was counted using a hand tally counter, and the results were recorded.

As shown in **Figure 3.4**, the cell counting process was done following the notion that only those cells touching the left and upper border lines were counted, while cells touching the right and bottom lines were not counted. This is to prevent the repeated counting of the same cells. The average number of live viable cells in each of the four grids was calculated. Then, the cell concentration was calculated using the following formula (Cell Signaling Technology, 2024).

Concentration of cells = average number of viable cells in four grids × 10^4 × dilution factor × original volume of cell suspension

Dilution factor = final volume / volume of cells

$$= \frac{100\ \mu L + 100\ \mu L}{100\ \mu L}$$

$$= 2$$

Volume of suspension required for seeding = number of cells required per well / cell concentration

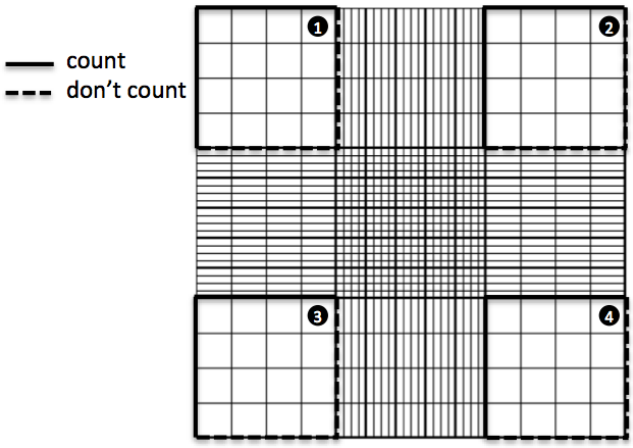

Figure 3.4: Grid lines of one chamber of a hemocytometer and the rule of cell counting (Adapted from Allevi, 2022).

3.7 MTT Assay

The master stock solutions of CuO NPs and cisplatin (used as the positive control) were made at a concentration of 5 mg/mL by dissolving 5 mg of each compound in 1 mL of DMSO. Subsequently, working solutions were prepared from these master stocks. Serial dilution of the master stock with Dulbecco's Modified Eagle Medium (DMEM) solution yielded seven sample solutions at concentrations of 1.56, 3.13, 6.25, 12.50, 25.00, 50.00, and 100.00 µg/mL.

Cells were seeded in a volume of 100 µL into the 96-well plate with 1×10^4 cells/well with DMEM. The cells were cultured for at least 24 hours at 37 °C, 5% CO_2 incubator for the purpose of growth and attachment of the monolayer cells. The following day, the plate was examined using an inverted microscope to confirm the attachment of cells. The cells in each well were treated with 100 µL of various concentrations of CuO NPs and cisplatin, respectively (**Figure 3.5**).

Wells with only cells and DMEM acted as negative controls, while the wells with only DMEM acted as blanks. The cells treated with cisplatin considered as the positive control of this experiment. The plate was placed in a 5% CO_2 incubator at 37 °C for 24 and 48 hours, respectively. The assay was conducted in triplicates for each sample, and each triplicate were divided into first run and second run.

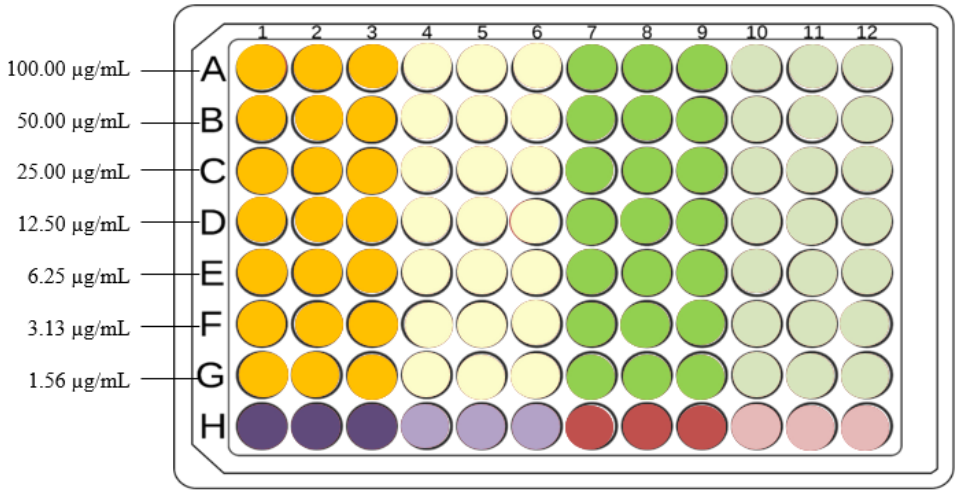

Figure 3.5: Layout of a 96-well plate for MTT assay.

Key:

First run:

- CuO NPs + cells + DMEM
- Cisplatin + cells + DMEM (positive control)
- Cells + DMEM (negative control)
- DMEM (blank)

Second run:

- CuO NPs + cells + DMEM
- Cisplatin + cells + DMEM (positive control)
- Cells + DMEM (negative control)
- DMEM (blank)

The cell viability was evaluated via the colorimetric MTT assay. After the end of each period of incubation, 20 µL of 5 mg/mL MTT reagent were added to all wells and incubated in darkness for 4 hours at 37 °C in a 5% CO_2 incubator. After 4 hours, the content from each well was completely removed, and 100 µL of 100% DMSO was added to dissolve and break down the purple formazan crystals. The plate was then incubated at room temperature for an additional 10 to 15 minutes. The cell viability was determined by measuring the absorbance spectrophotometrically at 570 nm using a microplate reader.

The data obtained were tabulated to calculate the percentage of cell viability. Graphs were generated by plotting the percentage of cell viability against different sample concentrations, and the IC_{50} values were determined from these graphs.

Calculation for cell viability (Karakas, Ari and Ulukaya, 2017):

$$\text{Percentage of cell viability} = \frac{X}{Y} \times 100\%$$

where,

X = average absorbance of treated cells

Y = average absorbance of negative controls

3.8 Statistical Analysis

Statistical analysis was performed to investigate the variance for various concentrations of green-synthesized *H. polyrhizus*-mediated CuO NPs and the positive control treated to the colon carcinoma (HCC2998) cells and Vero cells. The mean and standard deviation for the triplicates were calculated and tabulated. One-way ANOVA (IBM SPSS version 29.0) was implemented to analyze the significant cytotoxic effect of the green-synthesized CuO NPs at the significant level of p value < 0.05.

CHAPTER 4

RESULTS

4.1 Characterization of the Green-Synthesized CuO Nanoparticles

The black-colored powder obtained after calcination at 400 °C for 2 hours in the furnace was characterized by several instruments such as UV-Visible spectroscopy (UV-Vis), Fourier Transform Infrared Spectroscopy (FT-IR), Energy Dispersive X-ray Spectroscopy (EDX), X-ray Diffraction (XRD), and Scanning Electron Microscopy (SEM) to identify and confirm the size, morphology, crystallite nature, and to detect the probable functional groups in the green-synthesized *H. polyrhizus*-mediated CuO NPs.

4.1.1 UV-Visible Spectroscopy Analysis

The purpose of the UV-Vis spectroscopy analysis is to examine the absorption wavelength of the nanoparticles, especially to confirm the presence of reduced copper ions as CuO NPs. **Figure 4.1** depicts the UV-Visible absorption spectrum for the green-synthesized CuO NPs. Based on the graph plotted, the absorption peak can be detected at 286 nm. The band gap of CuO NPs is 4.15 eV as shown in the Tauc Plot presented in **Figure 4.2**.

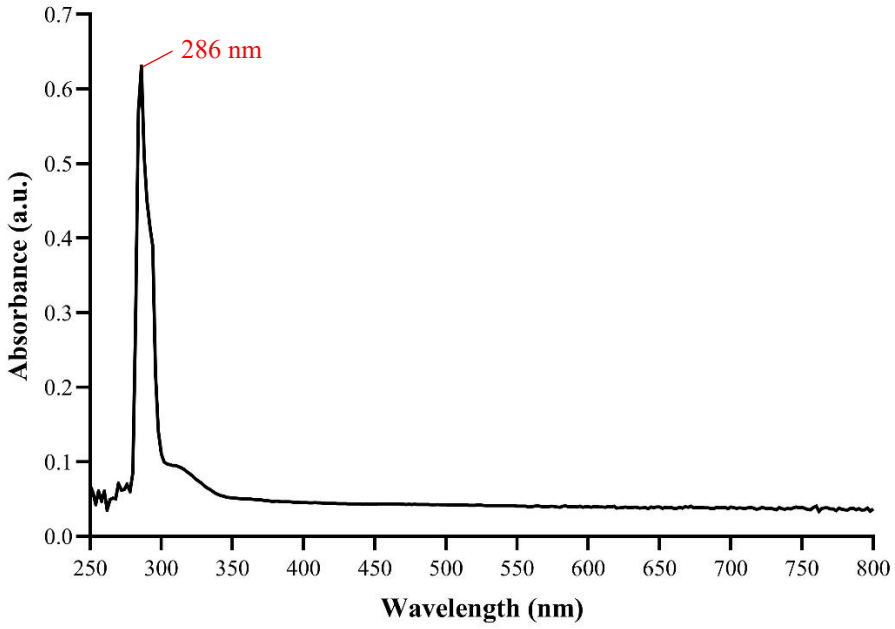

Figure 4.1: UV-Visible absorption spectrum of CuO NPs.

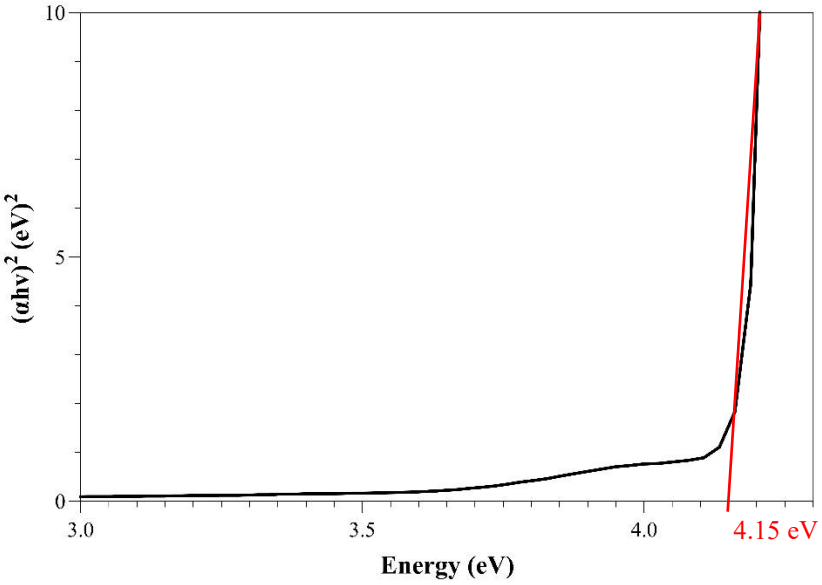

Figure 4.2: Band gap energy for the green-synthesized CuO NPs.

4.1.2 Field Emission Scanning Electron Microscopy Analysis

FE-SEM was utilized to obtain details of the size and to observe the surface morphology of the CuO NPs. **Figure 4.3a** shows the FE-SEM image for the CuO NPs photographed at 20000x magnification, whereas **Figure 4.3b** shows the morphology of the CuO NPs at 80000x magnification. The images revealed the spherical shape of CuO NPs in the presence of agglomeration. The size of the synthesized CuO NPs ranged from 24.9 to 35.4 nm.

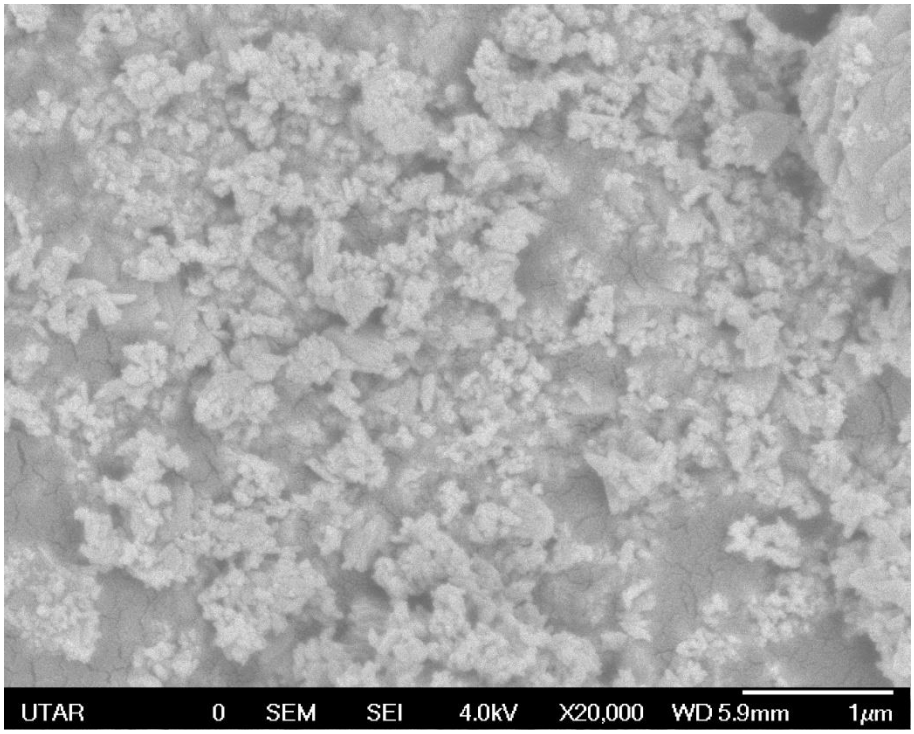

Figure 4.3a: Morphology of the CuO NPs under 20000x magnification.

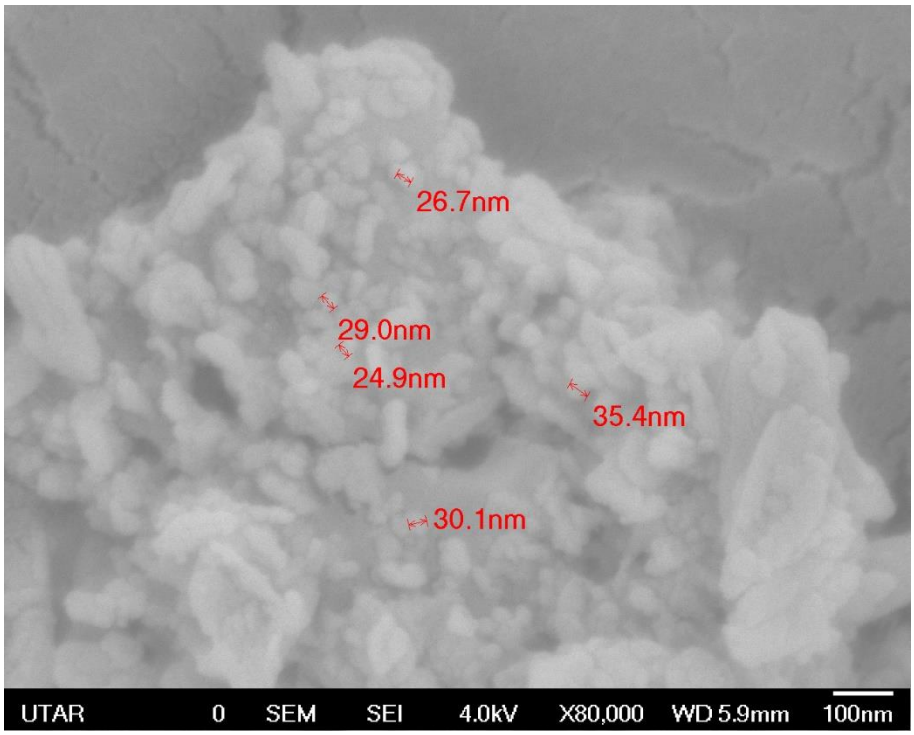

Figure 4.3b: Morphology of the CuO NPs under 80000x magnification.

4.1.3 Energy Dispersive X-ray Analysis

The EDX spectrum presented in **Figure 4.4** confirms the presence of the peaks attributed to copper and oxygen atoms in the green-synthesized CuO NPs, confirming the purity of the green-synthesized CuO NPs. However, tiny peaks of potassium ions were also detected because of the interactions with the *H. polyrhizus* plant extract during the process of bioprocessing. The weights percentage of the main elements found in CuO NPs are tabulated in **Table 4.1**.

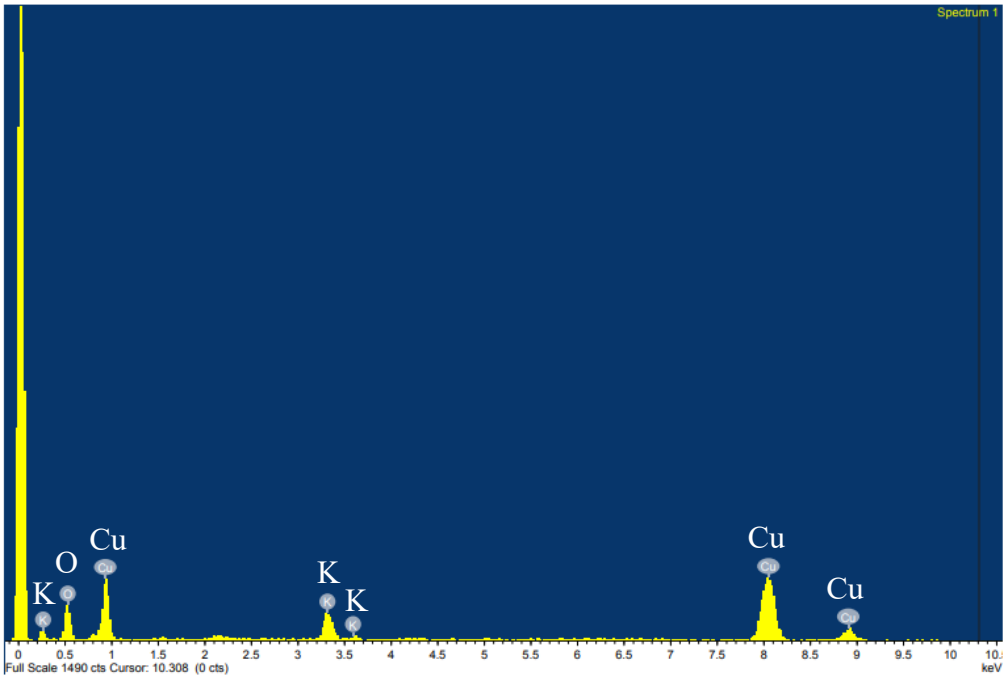

Figure 4.4: EDX spectrum of *H. polyrhizus*-mediated CuO NPs.

Table 4.1: Weight of the elements present in *H. polyrhizus*-mediated CuO NPs.

	Weight (%)		
	Cu	**O**	**K**
CuO NPs	62.59	31.82	5.59

4.1.4 X-ray Diffractometry Analysis

XRD analysis was performed to identify the crystal phases and crystallinity of the CuO NPs. The detected peaks for the CuO NPs with corresponding Miller indexes are plotted in **Figure 4.5**. The XRD analysis showed specific diffraction peaks at 2θ for the CuO NPs of 32.4, 35.5, 38.6, 48.7, 53.4, 58.2, 61.5, 66.2, 68.0, 72.3, and 75.2 degrees with corresponding Miller indexes of (110), (−111), (111), (−202), (020), (202), (−113), (−311), (220), (311), and (−222), respectively. These diffraction peaks agreed well with the standard card of The International Centre for Diffraction Data (ICDD) card No. 01-080-0076, confirming the monoclinic lattice structure of CuO NPs (Domyati, 2022; Kumar, et al., 2024). The crystal size of CuO NPs was determined using the Debye-Scherrer equation, resulting in a size of 23.62 nm (Sivagami and Asharani, 2022).

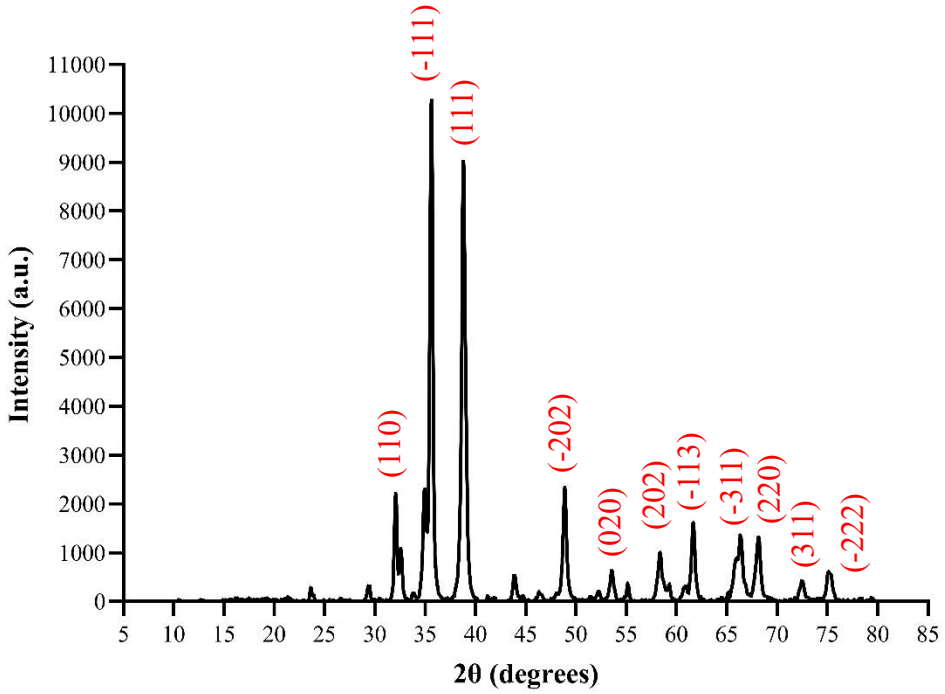

Figure 4.5: XRD patterns of *H. polyrhizus*-mediated CuO NPs from 10° to 80°.

Calculation of crystalline size by using Debye-Scherrer equation (Sivagami and Asharani, 2022)

To calculate β

$$\beta = \frac{FWHM\ in\ 2\theta \times \pi}{180°}$$

$$= \frac{0.3532 \times \pi}{180°}$$

$$= 6.1645 \times 10^{-3}$$

Debye-Scherrer Equation

$$D = \frac{k\lambda}{\beta\ cos\theta}$$

$$= \frac{0.9 \times 1.5406 \times 10^{-10}}{6.1645 \times 10^{-3} \cos 17.78°}$$

$$= 2.362 \times 10^{-8}\ \text{m}$$

$$= 23.62\ \text{nm}$$

where,

D = Mean size of nanoparticle

K = Scherrer constant (0.9)

λ = X-ray source wavelength (Cu-Kα radiation = 1.5406×10^{-10} m)

β = Diffraction broadening width at full-width half maximum (in radian 2θ)

θ = Bragg's diffraction angle

4.1.5 Fourier Transform Infrared Spectroscopy Analysis

FT-IR analysis was done to identify the possible significant functional groups found in the compound on the surface of the CuO NPs, which are responsible for reducing and capping agents. Based on the FTIR spectrum in **Figure 4.6**, the prominent absorption peak observed at 545 cm^{-1} was attributed to the Cu-O bond, thereby confirming the formation of CuO NPs. This assertion was corroborated by another high intensity peak at 1384 cm^{-1}, indicating the presence of Cu^{2+}-O^{2-} stretching mode. Additionally, a weak and broad peak detected at 3421 cm^{-1} corresponded to the O-H stretch, which is associated with hydrogen-bonded alcohols, suggesting the existence of water molecules that have been absorbed. The other possible functional groups that corresponded to each of the wavenumbers detected are listed in **Table 4.2**.

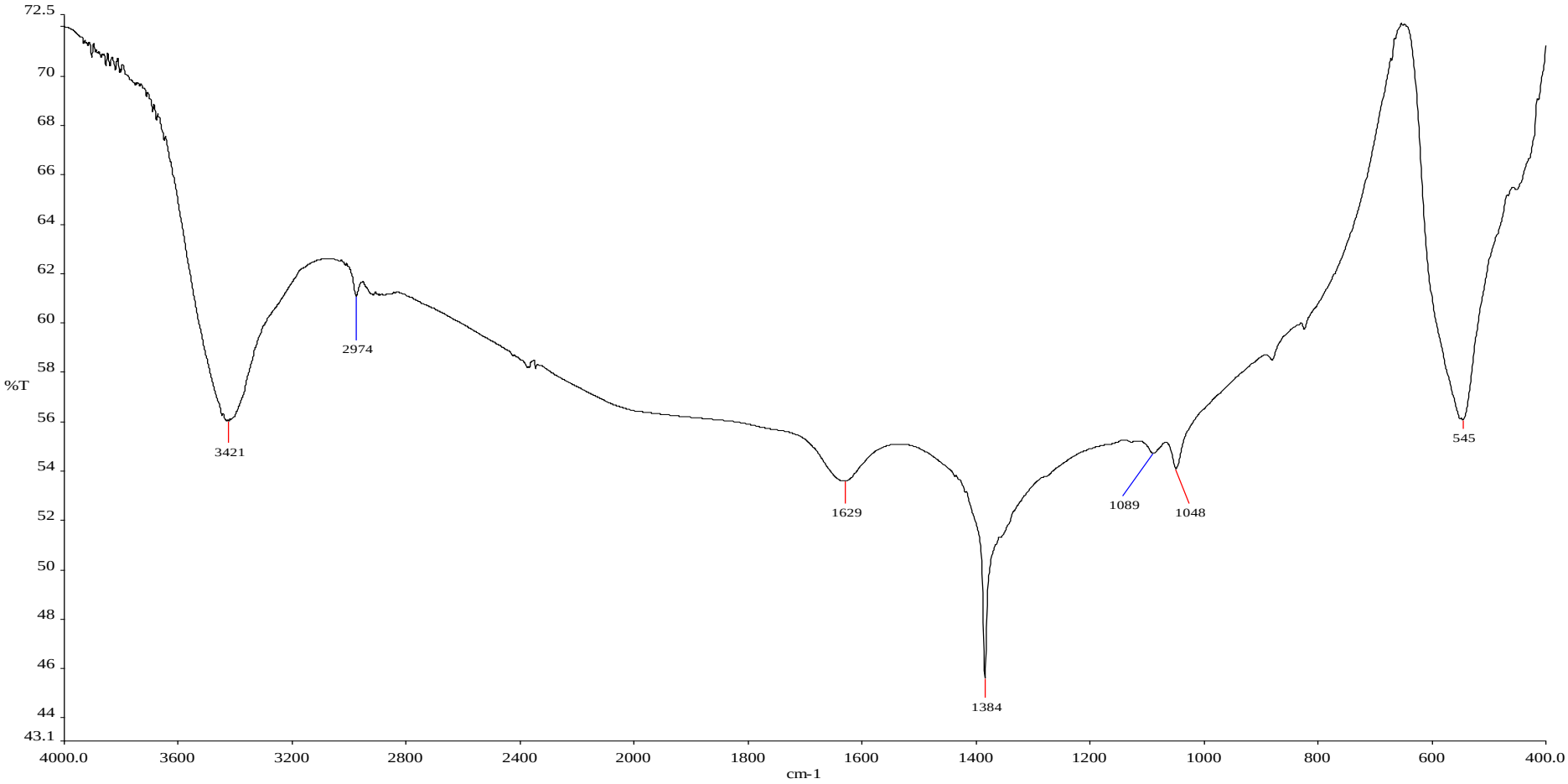

Figure 4.6: FT-IR spectrum for *H. polyrhizus*-mediated CuO NPs.

Table 4.2: FT-IR analysis on the molecular motion and possible functional groups present in the *H. polyrhizus*-mediated CuO NPs.

Wavenumber (cm^{-1})	Molecular Motion	Functional Group	Biomolecules
3421	O-H stretch	Hydroxyl group	Phenolic compound
2974	C-H stretch	Hydrocarbon	Alkanes
1629	C=C stretch	Carbonyl group	Flavonoids
1384	C-C stretch	Aromatic amine	Biogenic amines
1089, 1048	C-O stretch	Phenol	Flavonoids
545	Cu-O stretch	Cu-O	Inorganic compound

4.2 MTT Assay

4.2.1 HCC2998 Cells

The HCC2998 cell line originates from human colon carcinoma. The cells grow adherently and have the characteristics of epithelial-like morphology, as shown in **Figure 4.7**.

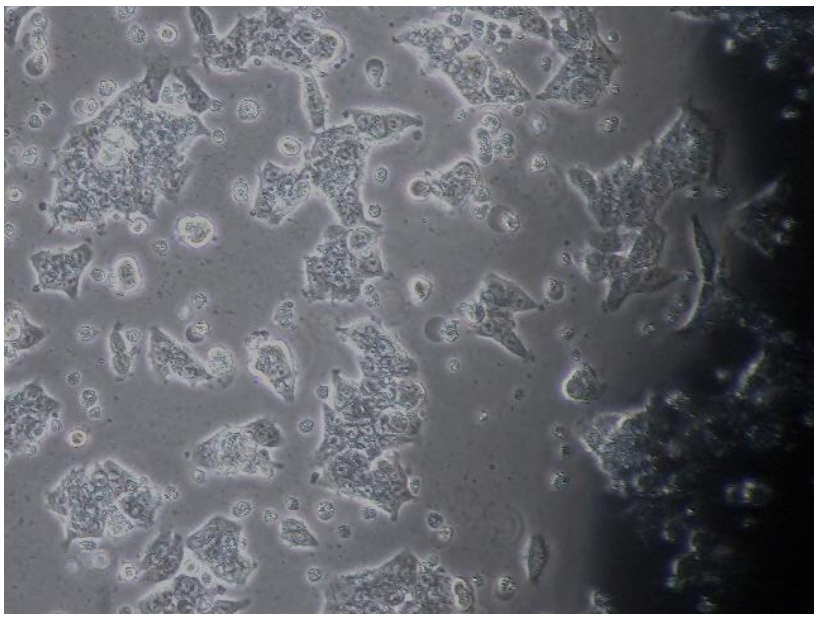

Figure 4.7: Morphology of HCC2998 cells cultured in CGM under 100x magnification.

The cytotoxic response of the green-synthesized CuO NPs was tested on colon carcinoma cells via MTT assay. The percentage of cell viability for HCC2998 cells after treatment with CuO NPs and cisplatin for 24- and 48-hours are tabulated in **Table 4.3** and **Table 4.4**, as well as **Figure 4.8** and **Figure 4.9**. Referring to the treatment of CuO NPs against colon cancer (HCC2998) cells after 24 hours incubation, the lowest cell viability treated with 100 µg/mL of CuO NPs and cisplatin were 52.35 ± 6.61% and 36.29 ± 1.94%, respectively. Upon 48 hours incubation, the lowest cell viability reduced to 41.46 ± 1.39% after treating the cells with 100 µg/mL of CuO NPs, and 21.65 ± 0.78% for cells treated with 100 µg/mL of cisplatin. Statistical analysis was conducted utilizing one-way ANOVA (IBM SPSS 29.0). The results indicated significant differences ($p < 0.05$) starting from 3.13 to 100.00 µg/mL of CuO NPs for 24 hours, and all the concentrations showed significant differences for 48 hours treatment of CuO NPs and cisplatin, as compared to the negative controls (untreated cells).

Additionally, the cellular structure and morphology was examined using an inverted microscope at 100x magnification for pre- and post-treatment of the cells. As shown in **Figures 4.10 and 4.11**, the non-treated HCC2998 cells showed a shiny appearance with a fibroblast-like epithelial shape, indicating viable cells (green arrows). However, the cell morphology changed from epithelial-shaped cells to irregular and rounded-shaped cells after treating the HCC2998 cells with both CuO NPs and cisplatin, respectively. Shrinkage of cells was observed, indicating apoptotic cells (red arrows).

Table 4.3: Percentage of cell viability of HCC2998 cells treated with various concentrations of CuO NPs and cisplatin with 24 hours treatment.

Concentrations (µg/mL)	Cell Viability (%)	
	CuO NPs	Cisplatin
0	100.00 ± 0.00	100.00 ± 0.00
1.56	93.75 ± 1.09	87.58 ± 2.49*
3.13	89.37 ± 1.86*	82.43 ± 6.83*
6.25	81.66 ± 1.45*	78.83 ± 5.15*
12.50	77.36 ± 1.88*	64.17 ± 3.57*
25.00	65.23 ± 3.48*	47.63 ± 3.49*
50.00	61.30 ± 4.80*	42.02 ± 0.94*
100.00	52.35 ± 6.61*	36.29 ± 1.94*

Data are presented as mean ± standard deviation from at least three independent experiments, * indicates statistically significant differences ($p < 0.05$).

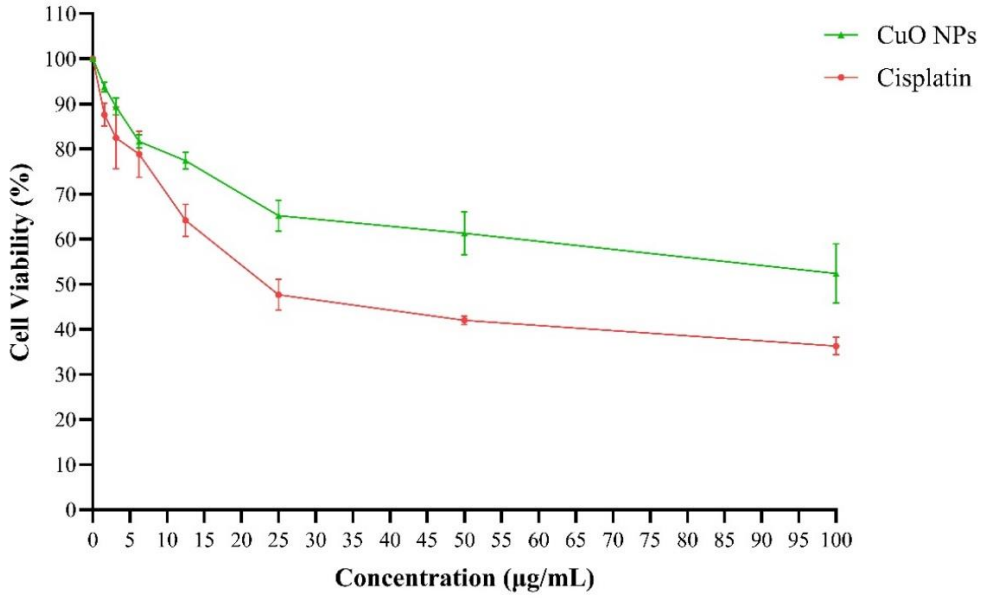

Figure 4.8: The percentage of cell viability of HCC2998 cells against different concentrations of CuO NPs and cisplatin at 24 hours incubation.

Table 4.4: Percentage of cell viability of HCC2998 cells treated with various concentrations of CuO NPs and cisplatin with 48 hours incubation.

Concentrations (µg/mL)	Cell Viability (%)	
	CuO NPs	Cisplatin
0	100.00 ± 0.00	100.00 ± 0.00
1.56	81.13 ± 2.44*	77.12 ± 4.27*
3.13	75.71 ± 1.39*	72.41 ± 3.42*
6.25	71.98 ± 2.91*	66.24 ± 4.08*
12.50	68.01 ± 0.63*	46.27 ± 4.57*
25.00	61.01 ± 1.97*	26.68 ± 0.14*
50.00	53.98 ± 1.67*	24.63 ± 1.34*
100.00	41.46 ± 1.39*	21.65 ± 0.78*

Data are presented as mean ± standard deviation from at least three independent experiments, * indicates statistically significant differences ($p < 0.05$).

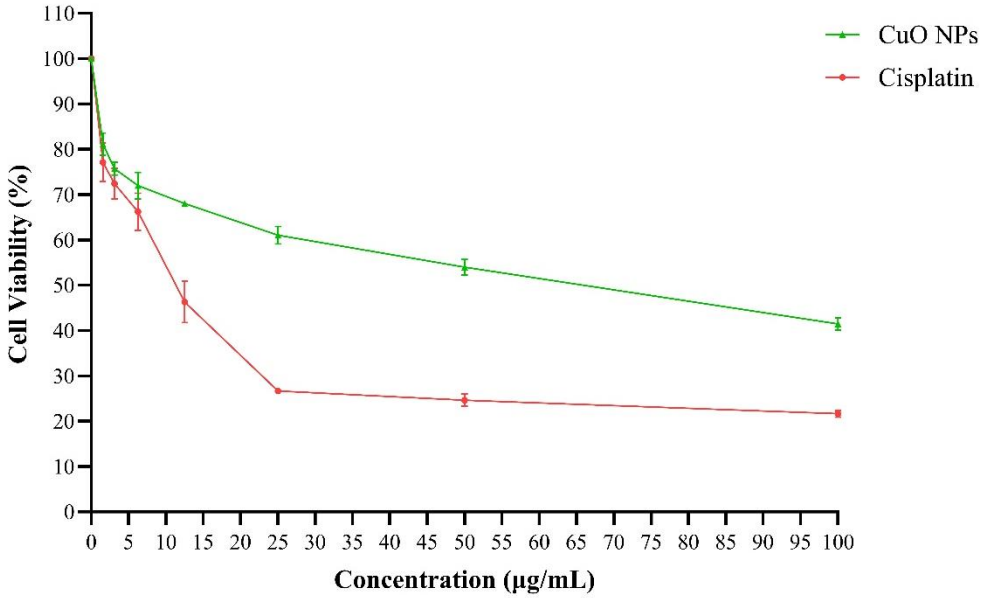

Figure 4.9: The percentage of cell viability of HCC2998 cells against different concentrations of CuO NPs and cisplatin at 48 hours incubation.

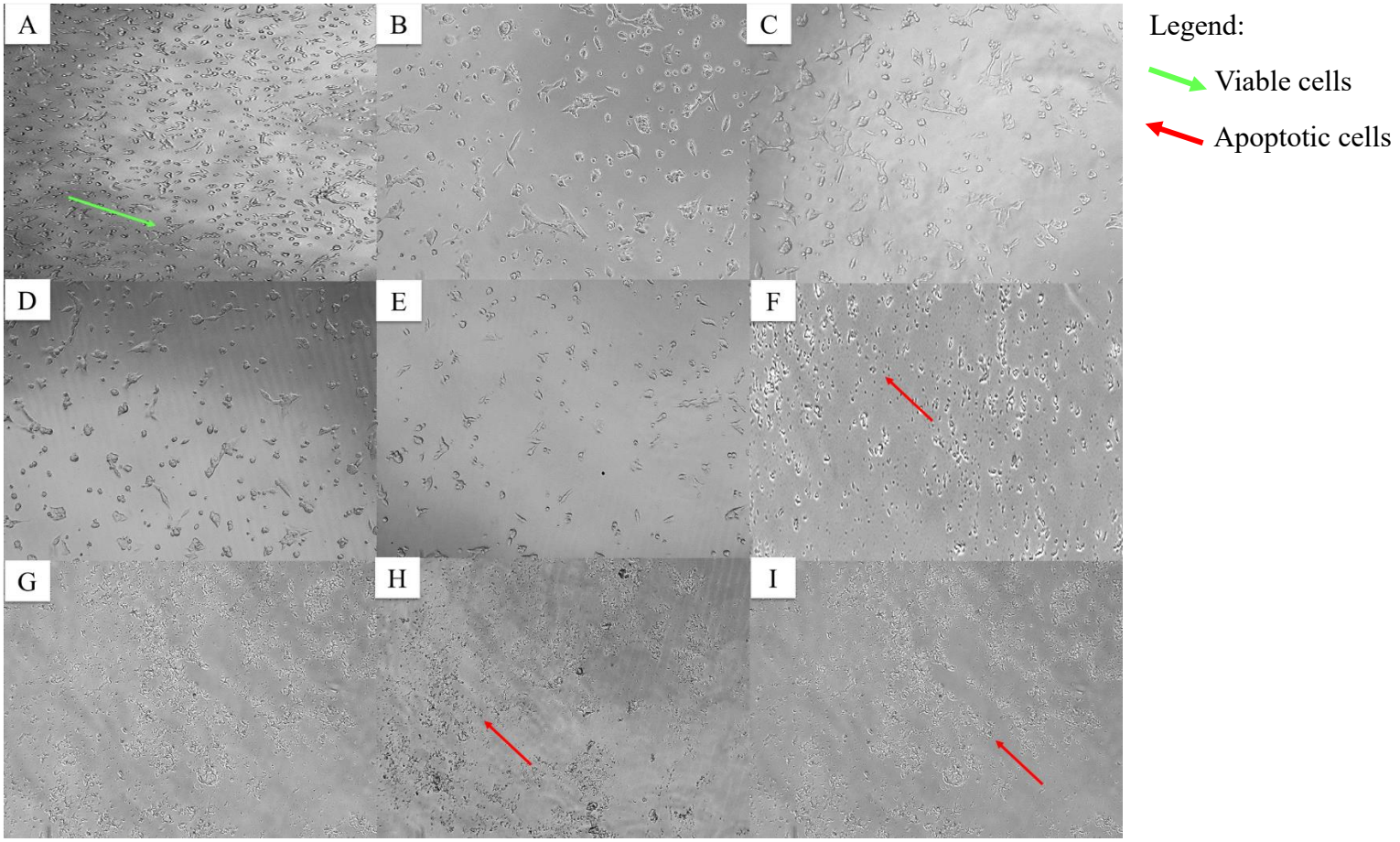

Figure 4.10: HCC2998 with various concentrations of CuO NPs after 24 hours under 100x magnification. (A) Negative control, (B) 1.56 µg/mL, (C) 3.13 µg/mL, (D) 6.25 µg/mL, (E) 12.50 µg/mL, (F) 25.00 µg/mL, (G) 50.00 µg/mL, (H) 100.00 µg/mL, (I) Positive control.

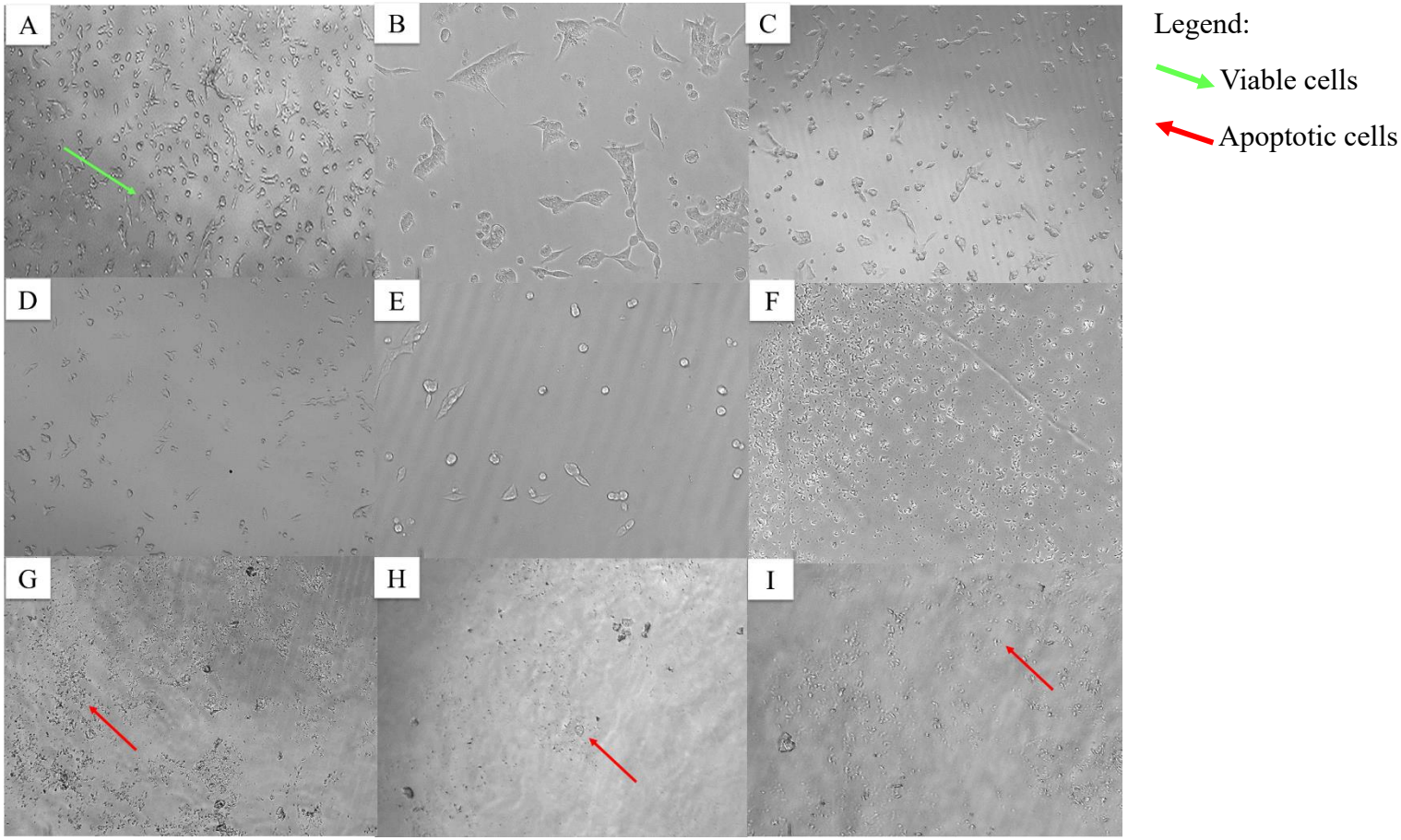

Figure 4.11: HCC2998 with various concentrations of CuO NPs after 48 hours under 100x magnification. (A) Negative control, (B) 1.56 µg/mL, (C) 3.13 µg/mL, (D) 6.25 µg/mL, (E) 12.50 µg/mL, (F) 25.00 µg/mL, (G) 50.00 µg/mL, (H) 100.00 µg/mL, (I) Positive control.

The IC_{50} values of CuO NPs and cisplatin were determined by graphical interpolation via GraphPad Prism 10 and are tabulated in **Table 4.5**. As the incubation period increased from 24 hours to 48 hours, the IC_{50} values for CuO NPs decreases from 14.61 ± 1.93 µg/mL to 7.45 ± 5.78 µg/mL. Meanwhile, cisplatin exhibited IC_{50} values from 12.52 ± 3.02 µg/mL to 7.61 ± 5.19 µg/mL. A lower IC_{50} value indicating higher potency of the drug (Berrouet, et al., 2022).

Table 4.5: IC_{50} values of *H. polyrhizus*-mediated CuO NPs treatment after 24- and 48-hours against HCC2998 cells.

Samples	**IC_{50} (µg/mL)**	
	24 hours	**48 hours**
CuO NPs	14.61 ± 1.93	7.45 ± 5.78
Cisplatin	12.52 ± 3.02	7.61 ± 5.19

Data are presented as mean ± standard deviation for at least three independent experiments.

4.2.2 Vero Cells

Figure 4.12 illustrates the characteristics of Vero cells, which are adherent cells with a fibroblast-like appearance and an elongated form.

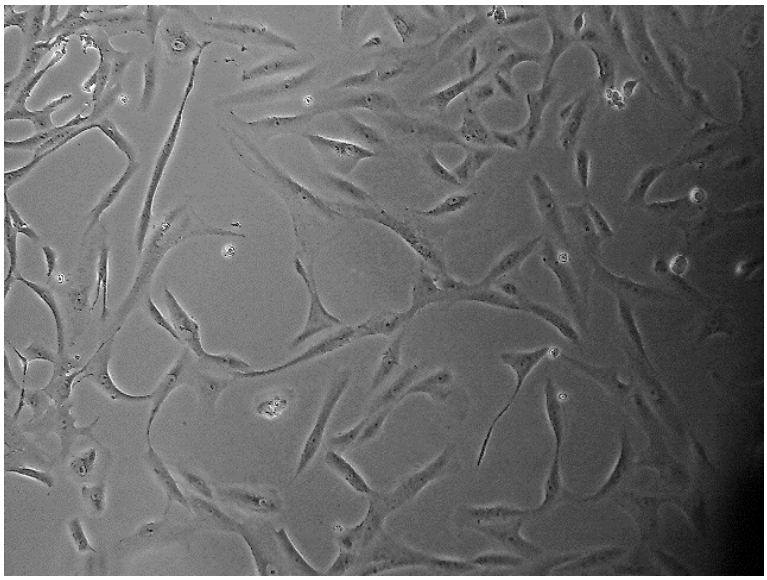

Figure 4.12: Morphology of the Vero cells cultured in CGM under 100x magnification.

The green-synthesized CuO NPs were tested on Vero cells via MTT reduction assay to assess the cytotoxicity. The percentage of cell viability for Vero cells after treatment with CuO NPs and DMSO for 24- and 48-hours incubation period are displayed in **Figure 4.13** and **Figure 4.14**. The results of the treatment of 100 µg/mL of CuO NPs with Vero cells following a 24 hours incubation revealed the lowest percentage of cell viability of 89.53 ± 0.73%, while the Vero cells treated with 100% DMSO had the lowest cell viability of 30.43 ± 1.20%. Besides, after treating the cells with 100 µg/mL of CuO NPs, the lowest cell viability after 48 hours of incubation was 82.06 ± 0.70%, while the percentage for cells treated with 100% DMSO was 8.61 ± 1.04%.

Statistical analysis was conducted using one-way ANOVA and the results highlighted significant differences ($p < 0.05$) at the concentrations of CuO NPs starting from 12.50 to 100.00 µg/mL for 24 hours. The concentrations of CuO NPs from 6.25 to 100.00 µg/mL showed significant differences in 48 hours treatment, as compared to the negative controls (untreated cells). DMSO, the positive control, showed significant differences for all concentrations at both 24- and 48-hours (**Table 4.6** and **Table 4.7**). Furthermore, IC_{50} values for CuO NPs against Vero cells cannot be determined from the plotted graph.

Table 4.6: Percentage of cell viability of Vero cells treated with various concentrations of CuO NPs and DMSO with 24 hours treatment.

Concentrations (µg/mL)	Cell Viability (%)	
	CuO NPs	DMSO
0	100.00 ± 0.00	100.00 ± 0.00
1.56	98.82 ± 0.50	67.49 ± 2.90*
3.13	97.82 ± 0.97	62.28 ± 0.91*
6.25	97.15 ± 0.72	51.24 ± 2.67*
12.50	95.09 ± 0.23*	41.67 ± 4.17*
25.00	92.42 ± 2.19*	37.80 ± 2.69*
50.00	91.16 ± 1.04*	35.23 ± 3.86*
100.00	89.53 ± 0.73*	30.43 ± 1.20*

Data are presented as mean ± standard deviation from at least three independent experiments, * indicates statistically significant differences ($p < 0.05$).

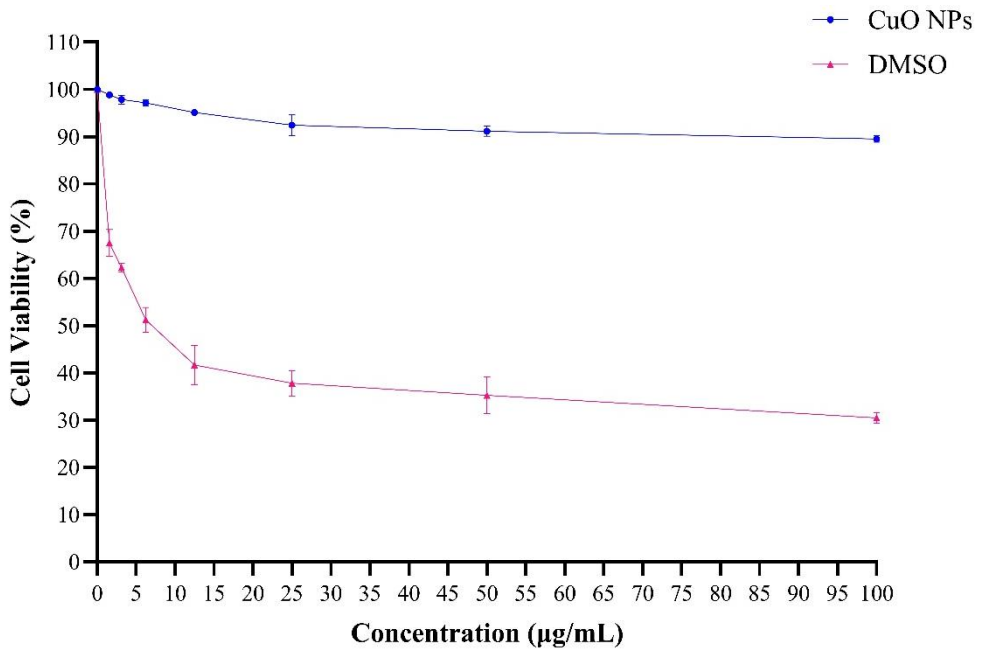

Figure 4.13: The percentage of cell viability of Vero cells against different concentrations of CuO NPs and DMSO at 24 hours incubation.

Table 4.7: Percentage of cell viability of Vero cells treated with various concentrations of CuO NPs and DMSO with 48 hours treatment.

Concentrations (µg/mL)	Cell Viability (%)	
	CuO NPs	Cisplatin
0	100.00 ± 0.00	100.00 ± 0.00
1.56	96.62 ± 0.36	45.75 ± 1.74*
3.13	94.37 ± 1.42	41.24 ± 1.93*
6.25	90.58 ± 1.32*	34.98 ± 3.81*
12.50	87.16 ± 0.46*	30.86 ± 0.62*
25.00	85.71 ± 0.26*	25.63 ± 2.89*
50.00	83.22 ± 2.67*	10.29 ± 1.27*
100.00	82.06 ± 0.70*	8.61 ± 1.04*

Data are presented as mean ± standard deviation from at least three independent experiments, * indicates statistically significant differences ($p < 0.05$).

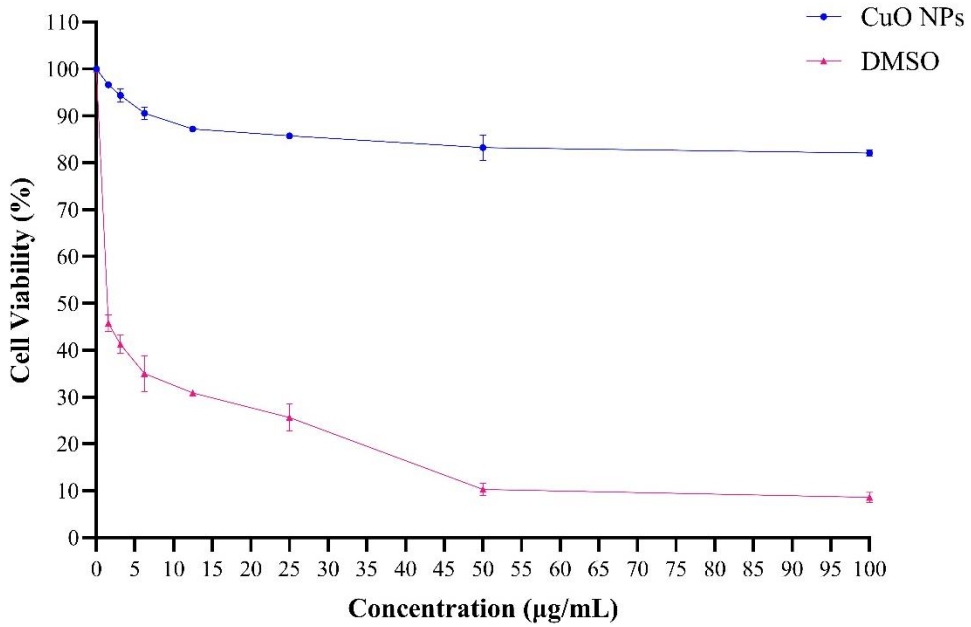

Figure 4.14: The percentage of cell viability of Vero cells against different concentrations of CuO NPs and DMSO at 48 hours incubation.

Additionally, the morphology of cells was observed under an inverted microscope at 100x magnification for pre- and post-treatment of the cells. According to **Figures 4.15 and 4.16**, a fibroblast-like elongated epithelial cells with a shiny appearance can be observed in the non-treated Vero cells (green arrows). However, the cell morphology changed from elongated-shaped cells to irregular and rounded-shaped cells after treating the Vero cells with highest concentration of CuO NPs and DMSO, respectively (red arrows).

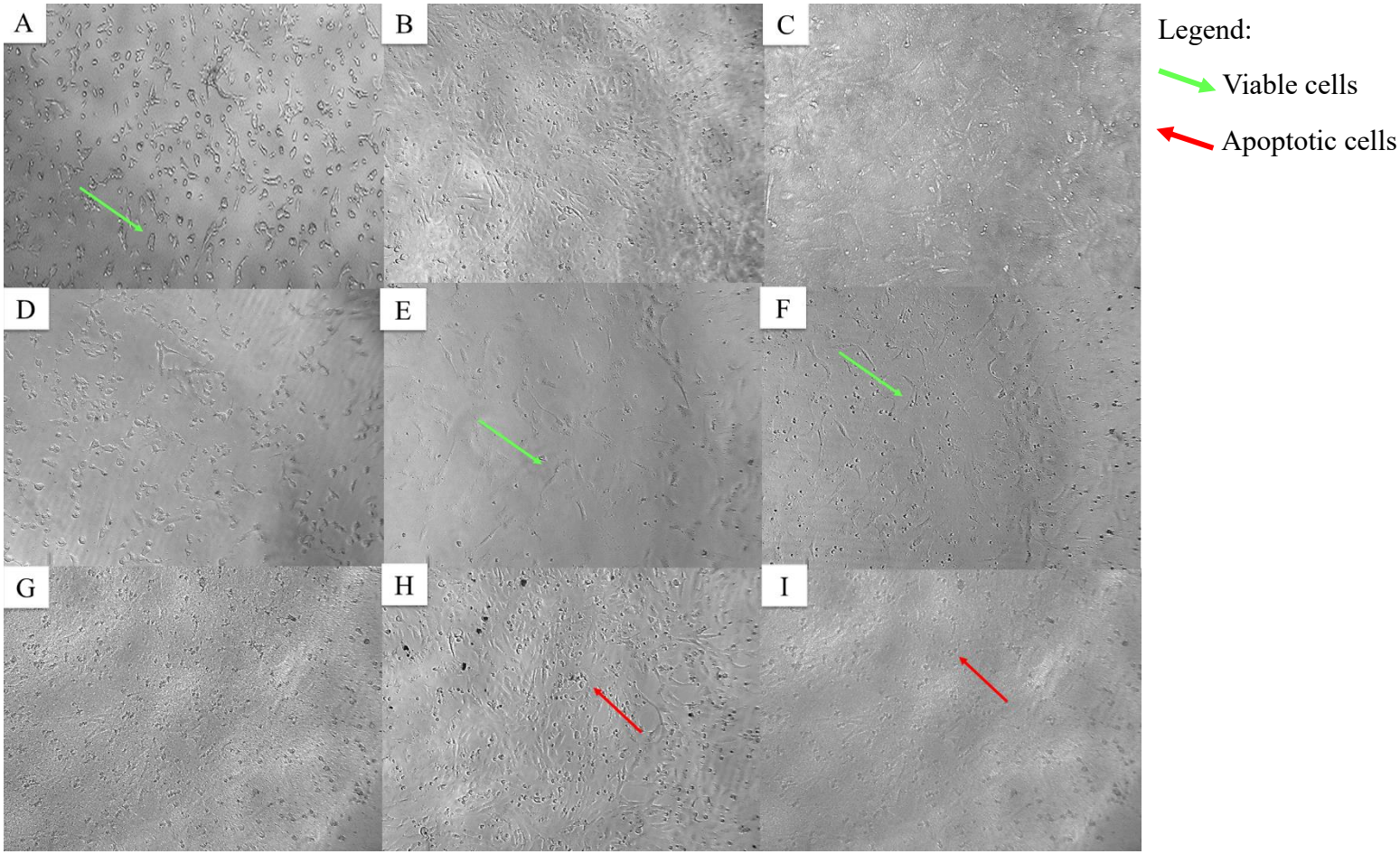

Figure 4.15: Vero cells with various concentrations of CuO NPs after 24 hours under 100x magnification. (A) Negative control, (B) 1.56 µg/mL, (C) 3.13 µg/mL, (D) 6.25 µg/mL, (E) 12.50 µg/mL, (F) 25.00 µg/mL, (G) 50.00 µg/mL, (H) 100.00 µg/mL, (I) Positive control.

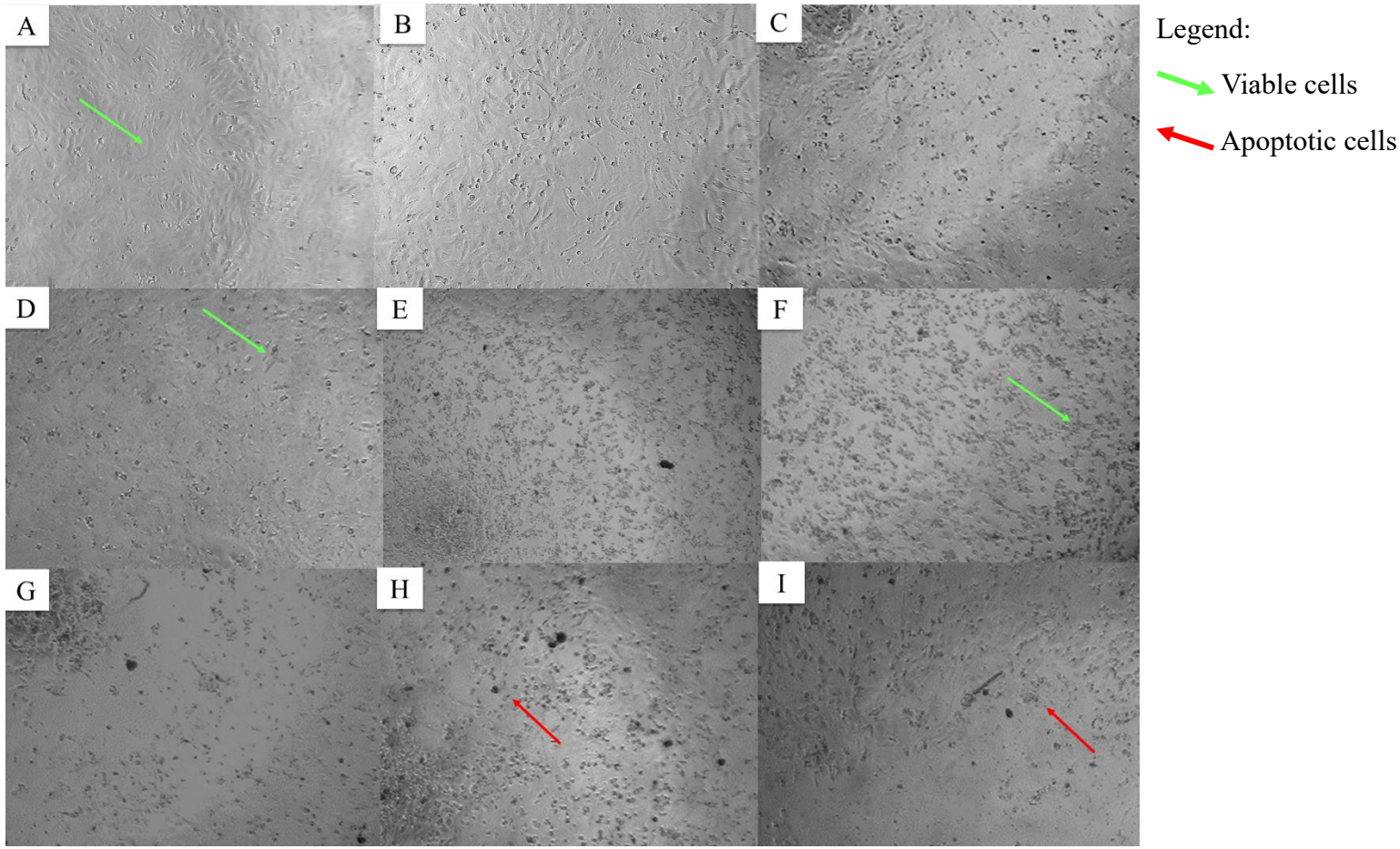

Figure 4.16: Vero cells with various concentrations of CuO NPs after 48 hours under 100x magnification. (A) Negative control, (B) 1.56 µg/mL, (C) 3.13 µg/mL, (D) 6.25 µg/mL, (E) 12.50 µg/mL, (F) 25.00 µg/mL, (G) 50.00 µg/mL, (H) 100.00 µg/mL, (I) Positive control.

CHAPTER 5

DISCUSSION

5.1 Characterization of the Green-Synthesized CuO NPs

5.1.1 Absorbance and Bandgap Energy

Based on the UV-Visible spectroscopy analysis, the absorbance of the green-synthesized CuO NPs was identified at the peak region of 286 nm. Similar peaks of 289 nm, 290 nm, and 291 nm were noted for the synthesized CuO NPs by Keabadile, et al. (2020). There is no other peak that can be observed in the whole spectrum, indicating that CuO NPs have successfully formed. UV-Visible spectroscopy is useful in detecting metal nanoparticles and characterize them based on size, shape, and stability. The localized surface plasmon resonance of metal nanoparticles allow for highly selective absorption of photons (Raja and Barron, 2024). The formation of the peak at that specific wavelength was due to surface plasmon resonance (SPR), which scatters light at different frequencies and absorbs light at similar frequencies. This was caused by these surface electrons all having a tendency to resonate at a single frequency. The vibration was detected as a result of the reaction between the emitted light photons and the conductivity of the electrons in the nanoparticles, which depends on the shape and dimensions of the nanoparticles. The result obtained was coherent with previous studies in which the synthesized CuO NPs showed surface plasmon resonance between 280 nm and 360 nm in the UV-Vis spectrum (Sankar, et al., 2014; Keabadile, et al., 2020; Satari, et al., 2021). Hence, it can be deduced that the green-synthesized nanoparticle was CuO NPs.

The disparity in energy levels between the valence and conduction bands is denoted as the band gap (Peymanfar, et al., 2020). In this study, the determination of band gap energy is critical because CuO NPs are made of semiconductor components. A Tauc plot can be illustrated with an association to the UV-Vis transmission spectrum by extrapolating the linear curves to the photon energy axis, which is the x-axis of the graph. As a result, the band gap energy for the green-synthesized *H. polyrhizus*-mediated CuO NPs determined from the Tauc plot was 4.15 eV. The band gap energy obtained in this study is closely related to the findings of Anjum, et al. (2023) and Divya (2019), who reported the band gap energies of 3.7 eV and 4.03 eV for the synthesized CuO NPs and pure CuO NPs, respectively. As the size of CuO NPs decreases, the band gap energy increases (Singh, Goyal and Devlal, 2018). Hence, the greater surface area of the CuO NPs will exhibit a better cytotoxic effect on the malignant cells in anticancer research.

5.1.2 Surface Morphology

The morphology of the green-synthesized CuO NPs was identified by the FE-SEM analysis. Based on the results obtained, the average sizes of the nanoparticles produced were smaller than 100 nm, which matched the nanosized characteristic of a nanoparticle (ranging from 1 to 100 nm). Apart from the sizes of CuO NPs, SEM images also revealed that all samples had a spherical shape, with indications of particle clustering. Previous studies had verified the spherical shape of CuO NPs (Amjad, et al., 2021; Altikatoglu, et al., 2017; Nzilu, et al., 2023). In previous study, SEM results of CuO NPs developed via green synthesis method also revealed that nanoparticles have a higher tendency to agglomerate

because of the high surface free energy and high rate of nucleation at high temperatures (Satari, et al., 2021; Putri, et al., 2023; Manjunatha, et al., 2021). Moreover, the aggregation of the green-synthesized CuO NPs would result from the sticky condition of the *H. polyrhizus* peels, which serves as the reducing and capping agent. This claim aligned with findings from other studies that highlighted sticky plant extract as a special characteristic (Mali, Raj and Trivedi, 2019; Chan, et al., 2022; Essa, 2024).

5.1.3 Elemental Compositions

EDX spectrum disclosed that the green-synthesized CuO NPs contain elements of copper (Cu), oxygen (O), and potassium (K). Based on the weight percentage of each element tabulated in **Table 4.1**, copper and oxygen were found to be 62.59% and 31.82%, respectively. The presence of Cu and O peaks in the EDX spectrum without any other elemental compositions indicates the successful formation of CuO NPs. However, small amounts (5.59%) of potassium were also detected due to the interaction with the plant extract during the process of bioprocessing. Moreover, several peaks for the same element can be observed. This phenomenon is caused by the stimulation of different atomic energy levels of the same element under the incident energy of the scanning electron microscope (SEM), suggesting several transitions of the same element (Gokul, 2020).

5.1.4 Crystallite Structure and Size

By examining the peaks' position and intensity with the XRD patterns of reference provided in the ICDD database, the observed diffraction peaks from XRD analysis suggested that the formation of green-synthesized CuO NPs was crystalline in nature with a monoclinic phase. The crystallite structure acquired was coherent with previous findings (Alhalili, 2022; Singh, et al., 2023). Besides, the XRD patterns did not show any additional peaks associated with secondary phases or impurities. There were also no discernible alterations in the diffraction angles or intensities. As a result, the calcination process results in high phase purity with the preferred components (Domyati, 2022).

Besides, the crystalline size of the nanoparticles was evaluated using a high intense Bragg's peak (Sivagami and Asharani, 2022). Debye-Scherrer equation was used to calculate the crystalline size of CuO NPs. At the highest diffraction peak of 35.62° in radian 2θ, the crystallite size was calculated to be 23.62 nm, which falls within the reported range of values, typically ranging from 14 to 25 nm (Keabadile, et al., 2020). As the crystalline size of the green-synthesized CuO NPs was within the range of 1 to 100 nm, it revealed that the CuO NPs were nanocrystalline.

5.1.5 Functional Groups

It has been observed that the width and intensity of peaks in an IR spectrum are directly influenced by particle size (Li, et al., 2019). As the particle size increases, the width of the peak narrows, accompanied by an increase in intensity (Amaro-Gahete, et al., 2019). Based on **Figure 4.6**, the peak at 545 cm^{-1} corresponds to

the Cu-O stretching vibration of CuO NPs in the monoclinic structure, indicating the successful synthesis of the CuO NPs (Varughese, Kaur and Singh, 2020). Other peaks observed in the FT-IR spectrum were due to the phytochemical components present in the *H. polyrhizus* peel extract.

The shortening in the absorption peak at 3421 cm^{-1} was attributed to the O-H stretching vibration of hydroxyl groups on the surface adsorbed by water molecules, indicating a reduction process of Cu^{2+} ions into colloidal Cu^{0} nanoparticles. A similar peak of 3419 cm^{-1} was reported by Dehaj and Mohiabadi (2019). Next, the presence of the peak at 2974 cm^{-1} represents C-H asymmetric stretching of alkanes. Previous study reported by Mohamed (2020) also presented their characterization peak of C-H stretching at the absorption peak position of 2921.72 cm^{-1}. The peaks seen at 1629 cm^{-1} and 1384 cm^{-1} show the C=O stretching of carbonyl group with the possible biomolecules of flavonoids and N-H stretching of aromatic amine, respectively. The strong band in the region between 1000 and 1300 cm^{-1} indicated a C-O stretching in the phenolic or alcoholic group. The presence of phenolic or alcoholic groups supported the claim that *H. polyrhizus* peel extract contains phytochemical compounds such as polyphenolics, alkaloids, and flavonoids, which have a significant impact on bio-reduction process of the synthesis of CuO NPs (Putri, et al., 2023).

Haruna, et al. (2022) conducted a similar study where they identified various functional groups present in the *H. polyrhizus*, including the -OH group at wavenumber 3381.21 cm^{-1}, C-H stretch at 2935.66 cm^{-1} and 775.38 cm^{-1}, C=O stretch at 1722.43 cm^{-1}, and C-O stretch at 1242.16 cm^{-1}.

5.2 Cytotoxic Effect of the *H. polyrhizus*-mediated CuO NPs

In MTT assay, two types of cells, namely Vero cells and HCC2998 cells, were used, which are the normal kidney cells and colon cancer cells, respectively. The aim of MTT assay in this research study was to investigate if cancer cells can be selectively killed off by the green-synthesized CuO NPs while normal cells are spared. This is in line with the goal of targeted therapy, in which the genes and proteins that are needed for cancer cells to survive and proliferate are targeted (Rosland and Engelsen, 2015). Nowadays, traditional chemotherapy, while effective at killing malignant cells, also damages normal cells, resulting in severe and undesirable side effects. Therefore, by developing therapies that target cancer cells specifically, it can minimize harm to our body's normal cells, mitigate adverse side effects and enhance the overall quality of life for individuals undergoing treatment (American Cancer Society, 2019; Liu, et al., 2015). In accordance with Mahmood, et al. (2022), there is evidence that suggests CuO NPs can target cancer cells without harming healthy, normal cells. Moreover, CuO NPs also demonstrated strong pro-apoptotic and antiproliferative effects on cancer cells that triggered cell death through apoptosis.

In this experiment, two incubation periods of treatment (24- and 48-hours) were applied to the cell lines. The activity of drug is heavily dependent on time. The duration of incubation impacts the accuracy of the cytotoxicity testing by affecting the assessment of cell viability, proliferation, and the cytotoxic impacts of substances on cells. As such, longer incubation periods would correspond better to dose toxicity, permitting a broader evaluation of the impacts of

treatments on cellular well-being and the dynamics of cytotoxicity (Gu, et al., 2018). By monitoring cells at different time points, the impacts of treatments on cellular viability and proliferation over time can be clearly observed and evaluated. These specific time points also allow researchers to monitor the response of cancer cells to different compounds at different stages of cell growth and division (Evans, et al., 2019).

Microscopic observation of colon cancer cells after 24- and 48-hours incubation without receiving any treatment showed a shiny epithelial appearance, indicating the cells were still alive and well-attached to the 96-well plate. In MTT assay, these cells act as a negative control to ensure there is no contamination for the assay. The addition of DMEM to the cells serves as a supportive and nourishing environment, which supplies the cells with essential nutrients and promotes cell growth and proliferation.

Based on **Figures 4.10 and 4.11**, colon cancer (HCC2998) cells treated with CuO NPs and cisplatin, respectively, manifested irregular or round-shaped cells, indicating the cells were dying and slowly detached from the 96-well plate. Cell shrinkage, which is also known as cellular atrophy, could be noticed under the inverted microscope, with several apoptotic bodies seen around the dying cells. According to Yu, et al. (2023), apoptotic bodies are a form of extracellular vesicles released by dying cells in the last stage of apoptosis. In apoptotic cell death, the cells divide into various apoptotic bodies, which is considered a morphological hallmark of apoptosis.

Besides, the black dots observed around the cells can be either the granules of cell components or the CuO NPs, given that the nanoparticles may target the malignant cells by ion channels or endocytosis (Cong, et al., 2021). As cancer cells contain a high concentration of anionic phospholipids on their surface, this unique feature will differentiate them from normal and healthy cells, hence attract the uptake of CuO NPs by malignant cells via endocytosis or ion channels. The excessive copper ions within cells will trigger the production of reactive oxygen species (ROS), leading to oxidative stress, which further leads to damage to the DNA and disrupts the mitochondrial membrane. Cuprous (Cu^{2+}) ions from the CuO NPs activate the autophagy and caspase pathways, leading to cell apoptosis (Siddiqui, et al., 2013; Shafagh, Rahmani and Delirezh, 2015; Aishajiang, et al., 2023).

As compared to the colon cancer cells treated with CuO NPs, the cells treated with cisplatin showed more dying cells that were detached from the 96-well plate with apoptotic bodies. Cisplatin is a potent first-line chemotherapy drug for patients diagnosed with various types of malignancies (Brown, Kumar and Tchounwou, 2019). Other than 5-fluorouracil, cisplatin stands out as one of the most frequently utilized chemotherapeutic agents for treating colon cancer. Hence, cisplatin was used as the positive control in this assay. The anticancer effectiveness of cisplatin is attributed to multiple mechanisms, including inhibition of DNA synthesis, creation of DNA lesions, and initiation of mitochondrial apoptosis through the formation of DNA adducts with platinum atoms (Jiang, et al., 2020). For instance, by directly targeting cells' DNA after entering the cancer cells, cisplatin limits the formation of tumors by creating a

cross-link between the guanine bases in DNA double-helix strands. As a result, DNA replication and transcription will be inhibited as the strands are now unable to be uncoiled and broken down, and so cell division is no longer possible and programmed cell death will occur (Drug Bank Online, 2005).

The percentage of cell viability with various concentrations of CuO NPs and cisplatin, respectively, are depicted in **Tables 4.3 and 4.4** and **Figures 4.8 and 4.9**. Based on **Figure 4.8** and **Figure 4.9**, the overall trend of the line graph demonstrated that CuO NPs, as well as cisplatin, showed dose-dependent toxicity against the cancer cells. Therefore, the decreasing trend in cell viability indicated that the cytotoxic activity on HCC2998 cells increased as the concentration of CuO NPs increased. This observation agrees with the research study by Gnanavel, Palanichamy and Roopan (2017) and Tabrez, et al. (2022) with significant anticancer cytotoxicity activity on colon carcinoma cell lines. Apart from that, Sedky, et al. (2024) revealed the lowest cell viability for HCT-116 cells at 15% for 100 µg/mL of CuO NPs treatment after 48 hours. The study conducted by Maithm, Khalid and Ahmed (2021) obtained the findings in which the cell viability decreased as the concentration of *O. cochinchinense* leaf extract-mediated CuO NPs exposed to HT-29 cells increased. Therefore, it proved that CuO NPs synthesized from different sources of reducing and capping agents will exert different effects on different lineages of cells.

The IC_{50} value is a quantitative measure of the concentration of a drug required to reduce a population of viable cells by 50%. IC_{50} is informative in measuring drug efficacy (potency). When the value of IC_{50} is low, it indicates that a minimal concentration of the drug is needed to achieve the desired inhibition (Berrouet, et al., 2020). Hence, in the development of drug and screening assays, a low IC_{50} value is considered favourable because it suggests that the drug is potent and effective at inhibiting the target. According to Widiandani, et al. (2023), as reported by the United States National Cancer Institute, a compound is categorized as highly cytotoxic if its IC_{50} value is below 20 µg/mL, moderate cytotoxic activity if IC_{50} falls between 21 and 200 µg/mL, mildly cytotoxic if the IC_{50} ranges from 201 and 500 µg/mL, and non-cytotoxic when IC_{50} greater than 500 µg/mL.

Using these standards as guidance, the green-synthesized *H. polyrhizus*-mediated CuO NPs with IC_{50} values of 14.61 ± 1.93 µg/mL (24 hours) and 7.45 ± 5.78 µg/mL (48 hours) show high cytotoxic activity at both 24- and 48-hours. Nevertheless, IC_{50} values of cisplatin at 12.52 ± 3.02 µg/mL (24 hours) and 7.61 ± 5.19 µg/mL (48 hours) were considered to have high cytotoxic activity. In contrast, IC_{50} values for CuO NPs against Vero cells cannot be determined accurately from the plotted graph. This is due to the reason that CuO NPs were not meant to kill the normal cells in the body, hence the lowest cell viability in the experiment was maintained above 50%.

Although the potential use of CuO NPs in cancer treatment has been proven in this study, it is also crucial to validate whether CuO NPs have the specificity of killing only cancer cells while sparing normal cells. Thus, Vero cells, which are the normal cells widely used in animal tissue culture that are isolated from African green monkey, have also been included in this study. DMSO, starting at 100%, followed by two-fold serial dilutions, was used as the positive control for Vero cells. Theoretically, DMSO – the cryoprotectant, is considered to be safe for almost all cells at low and appropriate concentrations, with low and no cytotoxicity to the cells, resulting in no significant decrease in cell viability (Life Tein, 2023). However, to compare cell viability with CuO NPs with the goal of sparing normal cells, high concentrations of DMSO that can exert cytotoxic effect on cells was used. This is to assess the potential cytotoxic effect of different compounds and to show notable variations in the lowest percentage of cell viability between cells treated with CuO NPs and DMSO for easier comparison.

According to **Figures 4.15 and 4.16**, most of the Vero cells showed shiny elongated fibroblast-like morphology, indicating healthy culture. This may be due to the reason that normal cells have an intact membrane, which restricts the entry of CuO NPs that have the potential to kill off the cells. The data tabulated in **Table 4.7** confirms that CuO NPs did not cause a substantial decrease in the viability of cells as compared to the cells treated with high percentages of DMSO. Vero cells treated with 100 µg/mL of CuO NPs still experienced the lowest cell viability of above 80%, whereas the lowest cell viability of Vero cells treated with 100% DMSO was 8.61%. By comparing the results obtained, the huge

differences in the lowest cell viability suggest that CuO NPs are considered to have a low cytotoxicity effect on normal cells.

Nowadays, the lack of ability of drug therapies to precisely recognize cancer cells is one of the primary barriers facing by the cancer chemotherapy (Padvi, et al., 2020). However, the outcomes obtained from this study are rather optimistic, as there is an apparent disparity between the percentage of cell viability for HCC2998 colon cancer cells and the Vero cell. Previous study reported by Prabu and Losettv (2024) found that the cell viability of Vero cells exposed to various concentrations of CuO NPs decreased slowly from 96.6% to 58.0%. DMSO-treated Vero cells showed a decreasing trend in cell viability as the percentage of DMSO used increased, and the lowest cell viability was recorded at 23% after 24 hours incubation (Aguilar, et al., 2002). In accordance with the research conducted by Sangour, et al. (2021), Ag NPs at the highest concentration of 100 µg/mL presented non-cytotoxic on Vero cells, while exhibiting a killing rate of 40% in MCF-7 breast cancer cells. These results suggest that different types of nanoparticles have their own unique variations that are selectively lethal to cancer cells rather than healthy cells because they can differentiate between the two types of cells in the body.

5.3 Limitations of the Study

The study of the reactive oxygen species (ROS) assay, which is useful to further study the role of ROS in killing cancer cells, was not carried out in this research study due to lack of facilities.

In MTT assay, Vero cells were used as the normal cells for cytotoxicity testing in comparison with HCC2998 colon carcinoma cells. However, Vero cells are kidney cell line isolated from African green monkey, while HCC2998 cells are highly differentiated human colon carcinoma cell line. Since both of the cell lines originate from different species, they may give rise to different cytotoxic effects. Hence, Vero cells may not represent a good model of normal human cell lines for toxicity testing.

5.4 Future Studies

ROS assay should be conducted after the MTT assay to further evaluate the level of ROS in cells following treatment with different concentrations of CuO NPs. It is crucial to study the ROS level, as the proposed mechanism of CuO NPs in killing malignant cells includes the factor of an increment in ROS level in the cells (Shafagh, Rahmani and Delirezh, 2015). Hence, by conducting ROS assay, the relationship between CuO NPs, ROS level, and the cytotoxic effect can be interlinked and well-studied to further confirm their respective roles in killing malignant cells.

Moreover, for a better comparison of the cytotoxic effect and anticancer activity of the green-synthesized *H. polyrhizus*-mediated CuO NPs, normal colon cell lines from humans should be chosen for a better understanding of the underlying mechanism. As only one type of cancer cell line was used in this study, more cell lines should be studied to provide a better knowledge of the anticancer activity. *In vivo* studies can also be performed to allow researchers to study the pharmacokinetics and pharmacodynamics of the potential anticancer drug within living organisms.

CHAPTER 6

CONCLUSIONS

CuO NPs were successfully produced using *Hylocereus polyrhizus* peel extract as a capping and reducing agent through the green synthesis process. The characterization confirmed the formation of CuO NPs. From the UV-vis spectroscopy analysis, a characteristic peak with a wavelength of 286 nm and a band gap energy of 4.15 eV was recorded for the CuO NPs synthesized through green methods. FE-SEM revealed the size of the spherical-shaped nanoparticles ranging from 24.9 to 35.4 nm in the presence of agglomeration. Peaks were attributed to copper, oxygen, and potassium atoms in the EDX spectrum. From the XRD analysis, monoclinic phase of CuO NPs was revealed, with a crystalline size of 23.62 nm. Based on the FTIR analysis, the possible phytochemical components detected in green-synthesized CuO NPs include the hydroxyl group, carbonyl group, aromatic amine, phenol, alcohol, and Cu-O, with the corresponding biomolecules of phenolic compounds, alkanes, flavonoids, biogenic amines, and inorganic compound. The green-synthesized CuO NPs exerted a higher cytotoxic effect towards colon cancer (HCC2998) cells, whereas CuO NPs showed lesser toxicity towards Vero cells. Cell viability was dose-dependent, with the most cell death at 100 µg/mL of CuO NPs in 48 hours for colon cancer cells. At the incubation period of 48 hours, CuO NPs showed the lowest IC_{50} value of 7.45 ± 5.78 µg/mL. However, CuO NPs did not exert significant cytotoxicity against Vero cells. This study shows the potential of *H. polyrhizus*-mediated CuO NPs to be utilized as a cytotoxic agent.

REFERENCES

AAT Bioquest, 2022. *MTT assay.* [online] Available at: <https://www.aatbio.com/resources/application-notes/mtt-assay> [Accessed 26 January 2024].

Abirami, K., Swain, S., Baskaran, V., Venkatesan, K., Sakthivel, K. and Bommayasamy, N., 2021. Distinguishing three dragon fruit (*Hylocereus* spp.) species grown in Andaman and Nicobar Islands of India using morphological, biochemical and molecular traits. *Scientific Reports*, [e-journal] 11, p. 2894. https://doi.org/10.1038/s41598-021-81682-x.

Aguilar, J.S., Roy, D., Ghazal, P. and Wagner, E.K., 2002. Dimethyl sulfoxide blocks herpes simplex virus-1 productive infection *in vitro* acting at different stages with positive cooperativity. Application of micro-array analysis. *BMC Infectious Diseases*, [e-journal] 2(1). http://dx.doi.org/10.1186/1471-2334-2-9.

Aishajiang, R., Liu, Z.S., Wang, T.J., Zhou, L. and Yu, D., 2023. Recent advances in cancer therapeutic copper-based nanomaterials for antitumor therapy. *Molecules*, [e-journal] 28(5), p. 2303. https://doi.org/10.3390%2Fmolecules28052303.

Alhalili, Z., 2022. Green synthesis of copper oxide nanoparticles CuO NPs from *Eucalyptus Globoulus* leaf extract: adsorption and design of experiments. *Arabian Journal of Chemistry*, [e-journal] 15(5), p. 103739. https://doi.org/10.1016/j.arabjc.2022.103739.

Alhalili, Z., 2023. Metal oxide nanoparticles: General structural description, chemical, physical, and biological synthesis methods, role in pesticides and heavy metal removal through wastewater treatment. *Molecules*, [e-journal] 28(7), p. 3086. https://doi.org/10.3390%2Fmolecules28073086.

Allevi, 2022. *Hemocytometer cell cpunting.* [online] Available at: <https://www.allevi3d.com/hemocytometer-cell-counting/> [Accessed 18 February 2024].

Altikatoglu, M., Attar, A., Erci, F., Cristache, C.M. and Isildak, I., 2017. Green synthesis of copper oxide nanoparticles using *Ocimum basilicum* extract and their antibacterial activity. *Fresenius Environmental Bulletin*, 26(12), pp. 7832-7837.

Amaro-Gahete, J., Benítez, A., Otero, R., Esquivel, D., Jimenez-Sanchidrian, C., Morales, J., Caballero, A. and Romero-Salguero, F.J., 2019. A comparative study of particle size distribution of graphene nanosheets synthesized by an ultrasound-assisted method. *Nanomaterials*, 9(2), p. 152.

American Cancer Society, 2019. *How chemotherapy drugs work.* [online] Available at: <https://www.cancer.org/cancer/managing-cancer/treatment-types/chemotherapy/how-chemotherapy-drugs-work.html> [Accessed 10 April 2024].

American Type Culture Collection, 2020. *Vero – CCL-81.* [online] Available at: <https://www.atcc.org/products/ccl-81> [Accessed 18 February 2024].

Aminuzzaman, M., Kei, L.M. and Liang, W.H., 2017. Green synthesis of copper oxide (CuO) nanoparticles using banana peel extract and their photocatalytic activities. *InAIP Conference Proceedings*, [e-journal] 1828(1), p. 020016. https://doi.org/10.1063/1.4979387.

Amjad, R., Mubeen, B., Ali, S.S., Imam, S.S., Alshehri, S., Ghoneim, M.M., Alzarea, S.I., Rasool, R., Ullah, I., Nadeem, M.S. and Kazmi, I., 2021. Green synthesis and characterization of copper nanoparticles using *Fortunella margarita* leaves. *Polymers*, [e-journal] 13(24), pp. 1-12. https://doi.org/10.3390/polym13244364.

Ammerman, N.C., Beier-Sexton, M. and Azad, A.F., 2009. Growth and maintenance of Vero cell lines. *Current Protocols in Microbiology*, [e-journal] 11(1), pp. 1-7. https://doi.org/10.1002%2F9780471729259.mca04es11.

Anjum, F., Shaban, M., Ismail, M., Gul, S., Bakhsh, E.M., Khan, M.A., Sharafat, U., Khan, S.B. and Khan, M.I., 2023. Novel synthesis of CuO/GO nanocomposites and their photocatalytic potential in the degradation of hazardous industrial effluents. *ACS Omega*, [e-journal] 8(20), pp. 17667-17681. https://doi.org/10.1021%2Facsomega.3c00129.

Awwad, A.M., Albiss, B.A. and Salem, N.M., 2015. Antibacterial activity of synthesized copper oxide nanoparticles using *Malva sylvestris* leaf extract. *SMU Medical Journal*, 2(1), pp. 91-101.

Badri, A., Slimi, S., Guergueb, M., Kahri, H. and Mateos, X., 2021. Green synthesis of copper oxide nanoparticles using prickly pear peel fruit extract: characterization and catalytic activity. *Inorganic Chemistry Communications*, [e-journal] 134, p. 109027. https://doi.org/10.1016/j.inoche.2021.109027.

Bao, Y.H., He, J., Song, K., Guo, J., Zhou, X.W. and Liu, S.M., 2021. Plant-extract-mediated synthesis of metal nanoparticles. *Journal of Chemistry*, [e-journal] 2021, pp. 1-14. https://doi.org/10.1155/2021/6562687.

Bayda, S., Adeel, M., Tuccinardi, T., Cordani, M. and Rizzolio, F., 2020. The history of nanoscience and nanotechnology: from chemical-physical applications to nanomedicine. *Molecules*, [e-journal] 25(1), p. 112. https://doi.org/10.3390%2Fmolecules25010112.

Bazzocco, S., Dopeso, H., Carton-Garcia, F., Macaya, I., Andretta, E., Chionh, F., Rodrigues, P., Garrido, M., Alazzouzi, H., Nieto, R., Sanchez, A., Schwartz, S., Bilic, J., Mariadason, J.M. and Arango, D., 2015. Highly expressed genes in rapidly proliferating tumor cells as new targets for colorectal cancer treatment. *Clinical Cancer Research: An Official Journal of the American Association for Cancer Research*, [e-journal] 21(16), pp. 3695-3704. https://doi.org/10.1158/1078-0432.CCR-14-2457.

Berrouet, C., Dorilas, N., Rejniak, K.A. and Tuncer, N., 2020. Comparison of drug inhibitory effects (IC_{50}) in monolayer and spheroid cultures. *Bulletin of Mathematical Biology*, [e-journal] 82(6), p. 68. https://doi.org/10.1007%2Fs11538-020-00746-7.

Brown, A., Kumar, S. and Tchounwou, P.B., 2019. Cisplatin-based chemotherapy of human cancers. *Journal of Cancer Science and Therapy*, 11(4), p. 97.

Cell Signaling Technology, 2024. *How to accurately count cells manually or with an automated cell counter.* [online] Available at: <https://blog.cellsignal.com/accurately-counting-cells-manually-or-with-an-automated-cell-counter> [Accessed 12 February 2024].

Chan, Y.B., Selvanathan, V., Tey, L.H., Akhtaruzzaman, M., Anur, F.H., Djearamane, S., Watanabe, A. and Aminuzzaman, M., 2022. Effect of calcination temperature on structural, morphological and optical properties of copper oxide nanostructures derived from *Garcinia mangostana L*. leaf extract. *Nanomaterials*, 12(20), pp. 3589–3608.

Cong, V.T., Tilley, R.D., Sharbeen, G., Phillips, P.A., Gaus, K. and Gooding, J.J., 2021. How to exploit different endocytosis pathways to allow selective delivery of anticancer drugs to cancer cells over healthy cells. *Chemical Science*, [e-journal] 12(46), pp. 15407-15417. https://doi.org/10.1039%2Fd1sc04656j.

Cytion, 2024. *Vero cell line – From viral research to vaccine development*. [online] Available at: <https://www.cytion.com/Knowledge-Hub/Cell-Line-Insights/Vero-Cell-Line-From-Viral-Research-to-Vaccine-Development/> [Accessed 18 February 2024].

Debela, D.T., Muzazu, S.G.Y., Heraro, K.D., Ndalama, M.T., Mesele, B.W., Haile, D.C., Kitui, S.K. and Manyazewal, T., 2021. New approaches and procedures for cancer treatment: *Current perspectives. SAGE Open Medicine*, [e-journal] 9(1). https://doi.org/10.1177%2F20503121211034366.

Dehaj, M.S. and Mohiabadi, M.Z., 2019. Experimental study of water-based CuO nanofluid flow in heat pipe solar collector. *Journal of Thermal Analysis and Calorimetry*, [e-journal] 137(1), pp. 2061-2072. http://dx.doi.org/10.1007/s10973-019-08046-6.

Desai, S.A., Sukhramani, P., Sukhramani, P.S., Tirthani, S.R. and Suthar, M.P., 2011. Biological cytotoxicity evaluation of spiro[azetidine-2, 3'-indole]-2', 4(1'H)- dione derivatives for anti-lung and anti-breast cancer activity. *Scholars Research Library*, 3(5), pp. 236-243.

Divakaran, D., Lakkakula, J. R., Thakur, M., Kumawat, M. K. and Srivastava, R., 2019. Dragon fruit extract capped gold nanoparticles: Synthesis and their differential cytotoxicity effect on breast cancer cells. *Materials Letters*, 236, pp. 498-502.

Divya, R., 2019. Effects of nyctanthes arbon-tristis leaf extract in the properties of CuO nanoparticles. *REST Journal on Emerging trends in Modelling and Manufacturing*, 5(2), pp. 32-36.

Domyati, D., 2022. Characterization of biofabrication copper (II) oxide nanoparticles and investigate the photocatalytic efficiency. *European Chemical Bulletin*, [e-journal] 11(2), pp. 1-6. https://doi.org/10.31838/ecb/2022.11.02.001.

Drug Bank Online, 2005. *Cisplatin.* [online] Available at: <https://go.drugbank.com/drugs/DB00515> [Accessed 11 April 2024].

Drug Discovery News, 2023. *Top instrument considerations for an MTT assay.* [online] Available at: <https://www.drugdiscoverynews.com/top-instrument-considerations-for-an-mtt-assay-15803> [Accessed 26 January 2024].

Essa, W.K., 2024. Methylene blue removal by copper oxide nanoparticles obtained from green synthesis of *Melia azedarach*: Kinetic and isotherm studies. *Chemistry*, [e-journal] 6(1), pp. 249-263. https://doi.org/10.3390/chemistry6010012.

Evans, D.M., Fang, J.W., Silvers, T., Delosh, R., Laudeman, J., Ogle, C., Reinhart, R., Selby, M., Bowles, L., Connelly, J., Harris, E., Krushkal, J., Rubinstein, L., Doroshow, J.H. and Teicher, B.A., 2019. Exposure time versus cytotoxicity for anticancer agents. *Cancer Chemotherapy and Pharmacology*, [e-journal] 84(2), pp. 359-371. https://doi.org/10.1007%2Fs00280-019-03863-w.

Fakhree, F.M., Waheed, I.F. and Mahmoud, K.M., 2021. Synthesis and characterization of CuO nanoparticles stabilized by quercetin and its application for anti-breast cancer activity. *Egyptian Journal of Chemistry*, 64(6), pp. 2989-2995.

Ferlay, J., Ervik, M., Lam, F., Laversanne, M., Colombet, M., Mery, L., Pineros, M., Znaor, A., Soerjomataram, I. and Bray, F., 2024. *Global cancer observatory: Cancer today.* [online] Available at: <https://gco.iarc.who.int/today> [Accessed 11 April 2024].

Foo, J.B., Ng, L.S., Lim, J.H., Tan, P.X., Lor, Y.Z., Loo, J.S.E., Low, M.L., Chan, L.C., Beh, C.Y., Leong, S.W., Yazan, L.S., Tor, Y.S. and How, C.W., 2019. Induction of cell cycle arrest and apoptosis by copper complex Cu(SBCM)2 towards oestrogen-receptor positive MCF-7 breast cancer cells. *RCS Advances*, [e-journal] 9, pp. 18359-18370. https://doi.org/10.1039/C9RA03130H.

Ghasemi, M., Turnbull, T., Sebastian, S. and Kempson, I., 2021. The MTT assay: utility, limitations, pitfalls, and interpretation in bulk and single-cell analysis. *International Journal of Molecular Sciences*, [e-journal] 22(23), p. 12827. https://doi.org/10.3390%2Fijms222312827.

Ghidan, A.Y., Al-Antary, T.M. and Awwad, A.M., 2016. Green synthesis of copper oxide nanoparticles using *Punica granatum* peels extract: effect on green peach Aphid. *Environmental Nanotechnology, Monitoring and Management*, [e-journal] 6(1), pp. 95-98. https://doi.org/10.1016/j.enmm.2016.08.002.

Gleneagles Hospitals, 2022. *Common cancer in Malaysia.* [online] Available at: <https://gleneagles.com.my/medical-specialties/oncology/cancer-statistics-malaysia> [Accessed 12 April 2024].

Global Biodiversity Information Facility, 2023. *Hylocereus polyrhizus (F.A.C.Weber) Britton & Rose.* [online] Available at: https://www.gbif.org/species/3944692 [Accessed 31 October 2023].

Gnanavel, V., Palanichamy, V. and Roopan, S. M., 2017. Biosynthesis and characterization of copper oxide nanoparticles and its anticancer activity on human colon cancer cell lines (HCT-116). *Journal of Photochemistry and Photobiology B: Biology*, 171, pp. 133-138.

Gokul, P., 2020. *Why does few peaks of the same element appear in different energy eV in EDX?* [online] Available at: <https://www.researchgate.net/post/Why_does_few_peaks_of_the_same_element_appear_in_different_energy_eV_in_EDX> [Accessed 20 April 2024].

Gu, X.L., Albrecht, W., Edlund, K., Kappenberg, F., Rahnenfuhrer, J., Leist, M., Moritz, W., Godoy, P., Cadenas, C., Marchan, R., Brecklinghaus, T., Pardo, L.T., Castell, J.V., Gardner, I., Han, B., Hengstler, J.G. and Stoeber, R., 2018. Relevance of the incubation period in cytotoxicity testing with primary human hepatocytes. *Archives of Toxicology*, [e-journal] 92(12), pp. 3505-3515. https://doi.org/10.1007/s00204-018-2302-0.

Gultekin, D.D., Nadaroglu, H., Gungor, A.A. and Kishali, N.H., 2017. Biosynthesis and characterization of copper oxide nanoparticles using Cimin grape (*Vitis vinifera cv.*) extract. *International Journal of Secondary Metabolite*, [e-journal] 4(3), pp. 77-84. https://doi.org/10.21448/ijsm.362672.

Hanahan, D. and Weinberg, R.A., 2011. Hallmarks of cancer: the next generation. *Cell*, [e-journal] 144(5), pp. 646-674. https://doi.org/10.1016/j.cell.2011.02.013.

Haruna, C.A., Malik, W.A., Rijal, M.Y.S., Watoni, A.H. and Ramadhan, L.O.A.N., 2022. Green synthesis of copper nanoparticles using red dragon fruit (*Hylocereus polyrhizus*) extract and its antibacterial activity for liquid disinfectant. *Journal of Scientific and Applied Chemistry*, 25(10), pp. 352-361.

Ijaz, F., Shahid, S., Khan, S.A., Ahmad, W. and Zaman, S., 2017. Green synthesis of copper oxide nanoparticles using *Abutilon indicum* leaf extract: antimicrobial, antioxidant and photocatalytic dye degradation activities. *Tropical Journal of Pharmaceutical Research*, [e-journal] 16(4), pp. 743-753. https://doi.org/10.4314/tjpr.v16i4.2.

Jiang, W., Yan, Y., Chen, M.Y., Luo, G.Y., Hao, J.J., Pan, J.J., Hu, S., Guo, P., Li, W.Y., Wang, R.Z., Zuo, Y., Sun, Y., Sui, S.L., Yu, W.D., Pan, Z., Zou, K., Zheng, Z.H., Deng, W.G., Wu, X.J. and Guo, W., 2020. Aspirin enhances the sensitivity of colon cancer cells to cisplatin by abrogating the binding of NF-κB to the COX-2 promoter. *Aging-US: Peer-Reviewed Aging Research Journal*, [e-journal] 12(1), pp. 611-627. https://doi.org/10.18632%2Faging.102644.

Karakas, D., Ari, F. and Ulukaya, E., 2017. The MTT viability assay yields strikingly false-positive viabilities although the cells are killed by some plant extracts. *Turkish Journal of Biology*, [e-journal] 41(6), pp. 919-925. https://doi.org/10.3906%2Fbiy-1703-104.

Keabadile, O.P., Aremu, A.O., Elugoke, S.E. and Fayemi, O.E., 2020. Green and traditional synthesis of copper oxide nanoparticles – Comparative study. *Nanomaterials*, [e-journal] 10(12), p. 2502. https://doi.org/10.3390/nano10122502.

Koteeswari, P., Sagadevan, S., Fatimah, I., Sibhatu, A.K., Razak, S.I., Leonard, E. and Soga, T., 2022. Green synthesis and characterization of copper oxide nanoparticles and their photocatalytic activity. *Inorganic Chemistry Communications*, [e-journal] 144, p. 109851. https://doi.org/10.1016/j.inoche.2022.109851.

Kumar, N., Upadhyay, S., Karthikeyan, M., Sen, A., Chetana, S., Joshi, N.C., Priyadarshi, N., Hossain, I. and Ansari, M.N.M., 2024. Facile one-step solid-state synthesis of CuO nanoparticles finely decorated over carbon sheets for improved OER activity. *Journal of Alloys and Compounds*, [e-journal] 983, p. 173842. https://doi.org/10.1016/j.jallcom.2024.173842.

Kumar, P.V., Shameem, U., Kollu, P., Kalyani, R.L. and Pammi, S.V., 2015. Green synthesis of copper oxide nanoparticles using Aloe vera leaf extract and its antibacterial activity against fish bacterial pathogens. *BioNanoScience*, [e-journal] 5(3), pp. 135-139. https://doi.org/10.1007/s12668-015-0171-z.

Li, X., Mei, Q., Chen, L., Zhang, H., Dong, B., Dai, X., He, C. and Zhou, J., 2019. Enhancement in adsorption potential of microplastics in sewage sludge for metal pollutants after the wastewater treatment process. *Water Research*, 157, pp. 228-237.

Life Tein, 2023. *DMSO usage in cell culture.* [online] Available at: <https://www.lifetein.com/chat/932729-DMSO-usage-in-cell-culture> [Accessed 31 March 2024].

Liu, B.Y., Ezeogu, L., Zellmer, L., Yu, B.F., Xu, N.Z. and Liao, D.Z.J., 2015. Protecting the normal in order to better kill the cancer. *Cancer Medicine*, [e-journal] 4(9), pp. 1394-1403. https://doi.org/10.1002%2Fcam4.488.

Mahmood, R.I., Kadhim, A.A., Ibraheem, S., Albukhaty, S., Mohammed-Salih, H.S., Abbas, R.H., Jabir, M.S., Mohammed, M.K.A., Nayef, U.M., AlMalki, F.A., Sulaiman, G.M. and Al-Karagoly, H., 2022. Biosynthesis of copper oxide nanoparticles mediated *Annona muricata* as cytotoxic and apoptosis inducer factor in breast cancer cell lines. *Scientific Reports*, 12, p. 16165. https://doi.org/10.1038/s41598-022-20360-y.

Mahmud, H., Raihan, T., Shakhik, T.Z., Khan, F.T. and Islam, M.T., 2023. Dragon fruit (*Hylocereus polyrhizus*): a green colorant for cotton fabric. *Colorants*, [e-journal] 2(2), pp. 230-244. https://doi.org/10.3390/colorants2020015.

Maithm, A.O., Khalid, H.H. and Ahmed, N., 2021. Biosynthesis of CuO NPs and its anticancer activity on human colon cancer cell lines (HT-29). *Journal of Physics: Conference Series*, [e-journal] 1963, p. 012151. https://doi.org/10.1088/1742-6596/1963/1/012151.

Mali, S.C., Raj, S. and Trivedi, R., 2019. Biosynthesis of copper oxide nanoparticles using *Enicostemma axillare (Lam.)* leaf extract. *Biochemistry and Biophysics Reports*, [e-journal] 20, p. 100699. https://doi.org/10.1016/j.bbrep.2019.100699.

Manjunatha, K.B., Bhat, R.S., Shashidhara, A., Kumar, H.S.A. and Nagashree, S., 2021. Antimicrobial and nonlinear optical studies of copper oxide nanoparticles. *Journal of Electronic Materials*, [e-journal] 50(16), pp. 3415-3421. http://dx.doi.org/10.1007/s11664-021-08838-3.

Mathew, N.S. and Negi, P.S., 2017. Traditional uses, phytochemistry and pharmacology of wild banana (*Musa acuminata Colla*): a review. *Journal of Ethnopharmacology*, [e-journal] 196, pp. 124-140. https://doi.org/10.1016/j.jep.2016.12.009.

Mayo Clinic, 2022. *Cancer – Symptoms and causes.* [online] Available at: <https://www.mayoclinic.org/diseases-conditions/cancer/symptoms-causes/syc-20370588> [Accessed 6 February 2024].

Meerloo, J., Kaspers, G.J.L. and Cloos, J., 2011. Cell sensitivity assays: The MTT assay. *Methods in Molecular Biology*, [e-journal] 731, pp. 237-245. https://doi.org/10.1007/978-1-61779-080-5_20.

Messaoudi, O. and Bendahou, M., 2020. Biological synthesis of nanoparticles using Endophytic microorganisms: current development. *Nanotechnology and the Environment*, [e-journal] 1. http://dx.doi.org/10.5772/intechopen.93734.

Miranda-Castro, S.P., 2016. Application of chitosan in fresh and minimally processed fruits and vegetables. *Chitosan in the Preservation of Agricultural Commodities*, [e-journal] pp. 67-113. http://dx.doi.org/10.1016/B978-0-12-802735-6.00003-3.

Mohamed, E.A., 2020. Green synthesis of copper and copper oxide nanoparticles using the extract of seedless dates. *Heliyon*, [e-journal] 6, p. 03123. https://doi.org/10.1016/j.heliyon.2019.e03123.

Muhammad, N.W.F., Nurrulhidayah, A.F., Hamzah, M.S., Rashidi, O. and Rohman, A., 2020. Physiochemical properties of dragon fruit peel pectin and citrus peel pectin: a comparison. *Food Research*, [e-journal] 4(1), pp. 266-273. https://doi.org/10.26656/fr.2017.4(S1).S14.

National Cancer Institute, 2015. *Cell lines in the In Vitro screen.* [online] Available at: <https://dtp.cancer.gov/discovery_development/nci-60/cell_list.htm> [Accessed 19 February 2024].

National Cancer Institute, 2021. *What is cancer?* [online] Available at: <https://www.cancer.gov/about-cancer/understanding/what-is-cancer#:~:text=Cancer%20is%20a%20disease%20caused,are%20also%20called%20genetic%20changes.> [Accessed 13 April 2024].

Nishikito, D.F., Borges, A.C.A., Laurindo, L.F., Otoboni, A.M.M.B., Direito, R., Goulart, R.A., Nicolau, C.C.T., Fiorini, A.M.R., Sinatora, R.V. and Barbalho, S.M., 2023. Anti-inflammatory, antioxidant, and other health effects of dragon fruit and potential delivery systems for its bioactive compounds. *Pharmaceutics*, [e-journal] 15(1), p. 159. https://doi.org/10.3390%2Fpharmaceutics15010159.

Nzilu, D.M., Madivoli, E.S., Makhanu, D.S., Wanakai, S.I., Kiprono, G.K. and Kareru, P.G., 2023. Green synthesis of copper oxide nanoparticles and its efficiency in degradation of rifampicin antibiotic. *Scientific Reports*, [e-journal] 13, p. 14030. https://doi.org/10.1038/s41598-023-41119-z.

Okpara, E.C., Ogunjinmi, O.E., Oyewo, O.A., Fayemi, O.E. and Onwudiwe, D.C., 2021. Green synthesis of copper oxide nanoparticles using extracts of *Solanum macrocarpon* fruit and their redox responses on SPAu electrode. *Heliyon*, [e-journal] 7(12), pp. 1-13. https://doi.org/10.1016/j.heliyon.2021.e08571.

Padvi, M.N., Hiremath, N.G., Prasad, S.R.D., Nayak, A.K., Bohara, R.A., Attrar, Y., Ramteke, A.A. and Sarvalkar, P., 2020. *Bos taurus* urine assisted biosynthesis of CuO nanomaterials: A new paradigm of antimicrobial and antineoplastic therapy. *Macromolecular Symposia*, [e-journal] 392, p. 1900172. http://dx.doi.org/10.1002/masy.201900172.

Pansambal, S., Gavande, S., Ghotekar, S., Oza, R. and Deshmukh, K., 2017. Green synthesis of CuO nanoparticles using *Ziziphus mauritiana L.* extract and its characterizations. *International Journal of Scientific Research in Science and Technology*, 3(8), pp. 1388-1392.

Peymanfar, R., Yektaei, M., Javanshir, S. and Selseleh-Zakerin, E., 2020. Regulating the energy band-gap, UV–Vis light absorption, electrical conductivity, microwave absorption, and electromagnetic shielding effectiveness by modulating doping agent. *Polymer*, [e-journal] 209, p. 122981. https://doi.org/10.1016/j.polymer.2020.122981.

Phebe, D., Chew, M.K., Suraini, A.A., Lai, O.M. and Janna, O.A., 2009. Red-fleshed pitaya (*Hylocereus polyrhizus*) fruit colour and betacyanin content depend on maturity. *International Food Research Journal*, 16(1), pp. 233-242.

Prabu, P. and Losetty, V., 2024. Green synthesis of copper oxide nanoparticles using *Macroptilium Lathyroides (L)* leaf extract and their spectroscopic characterization, biological activity and photocatalytic dye degradation study. *Journal of Molecular Structure*, [e-journal] 1301, p. 137404. https://doi.org/10.1016/j.molstruc.2023.137404.

Priya, M., Venkatesan, R., Deepa, S., Sana, S.S., Arumugam, S., Karami, A.M., Vetcher, A.A. and Kim, S.C., 2023. Green synthesis, characterization, antibacterial, and antifungal activity of copper oxide nanoparticles derived from *Morinda citrifolia* leaf extract. *Scientific Reports*, [e-journal] 13, p. 18838. https://doi.org/10.1038/s41598-023-46002-5.

Putri, S.E., Herawati, N., Fudhail, A., Pratiwi, D.E., Side, S., Rahman, A., Desa, S.S., Ahmad, N., Junaedi, S. and Surleva, A., 2023. Biosynthesis of copper nanoparticles using *Hylocereus costaricensis* peel extract and their photocatalytic properties. *Karbala International Journal of Modern Science*, [e-journal] 9(2), pp. 289-306. https://doi.org/10.33640/2405-609X.3300.

Raja, P.M.V. and Barron, A. R., 2024. *8.5: Spectroscopic characterization of nanoparticles.* Available at: <https://chem.libretexts.org/Bookshelves/Analytical_Chemistry/Physical_Methods_in_Chemistry_and_Nano_Science_(Barron)/08%3A_Structure_at_the_Nano_Scale/8.05%3A_Spectroscopic_Characterization_of_Nanoparticles> [Accessed 24 March 2024].

Rajagopal, G., Nivetha, A., Sundar, M., Panneerselvam, T., Murugesan, S., Parasuraman, P., Kumar, S., Ilango, S. and Kunjiappan, S., 2021. Mixed phytochemicals mediated synthesis of copper nanoparticles for anticancer and larvicidal applications. *Heliyon*, 7, pp. 1-15.

Ramasubbu, K., Padmanabhan, S., Al-Ghanim, K.A., Nicoletti, M., Govindarajan, M., Sachivkina, N. and Rajeswari, V. D., 2023. Green synthesis of copper oxide nanoparticles using *Sesbania grandiflora* leaf extract and their evaluation of anti-diabetic, cytotoxic, anti-microbial, and anti-inflammatory properties in an *in-vitro* approach. *Fermentation*, [e-journal] 9(4), p. 332. https://doi.org/10.3390/fermentation9040332.

Riss, T., 2024. *Is your MTT assay really the best choice?* [online] Available at: <https://worldwide.promega.com/resources/pubhub/is-your-mtt-assay-really-the-best-choice/> [Accessed 26 January 2024].

Rosland, G.V. and Engelsen, A.S.T., 2015. Novel points of attack for targeted cancer therapy. *Basic and Clinical Pharmacology and Toxicology*, [e-journal] 116(1), pp. 9-18. https://doi.org/10.1111%2Fbcpt.12313.

Saneto, 2012. *Hylocereus polyrhizus.* [online] Available at: <http://darsatop.lecture.ub.ac.id/2015/06/buah-naga-merah-hylocereus-polyrhizus/> [Aceesed 3 February 2024].

Sangour, M.H., Ali, I.M., Atwan, Z.W. and Ali, A.A.L., 2021. Effect of Ag nanoparticles on viability of MCF-7 and Vero cell lines and gene expression of apoptotic genes. *Egyptian Journal of Medical Human Genetics*, [e-journal] 22, p. 9. https://doi.org/10.1186/s43042-020-00120-1.

Sankar, R., Manikandan, P., Malarvizhi, V., Fathima, T., Shivashangari, K.S. and Ravikumar, V., 2014. Green synthesis of colloidal copper oxide nanoparticles using Carica papaya and its application in photocatalytic dye degradation. *Spectrochimica Acta Part A: Molecular and Biomolecular Spectroscopy*, [e-journal] 121, pp. 746-750. https://doi.org/10.1016/j.saa.2013.12.020.

Satari, C., Sidqi, R.S., Putra, R.F., Putri, S.R. and Nandiyanto, A.B.D., 2021. Literature review: synthesis of CuO (copper oxide) nanoparticles for thermal energy storage. *International Journal of Energetica*, 6(2), pp. 21-34.

Sedky, N.K., Fawzy, I.M., Hassan, A., Mahdy, N.K., Attia, R.T., Shamma, S.N., Alfaifi, M.Y., Elbehairi, S.E., Mokhtar, F.A. and Fahmy, S.A., 2024. Innovative microwave-assisted biosynthesis of copper oxide nanoparticles loaded with platinum(II) based complex for halting colon cancer: cellular, molecular, and computational investigations. *RSC Advances*, [e-journal] 14(1), pp. 4005-4024. https://doi.org/10.1039/D3RA08779D.

Shafagh, M., Rahmani, F. and Delirezh, N., 2015. CuO nanoparticles induce cytotoxicity and apoptosis in human K562 cancer cell line via mitochondrial pathway, through reactive oxygen species and P53. *Iranian Journal of Basic Medical Sciences*, [e-journal] 18(10), pp. 993-1000. https://pubmed.ncbi.nlm.nih.gov/26730334.

Shyamalagowri, S., Charles, P., Manjunathan, J., Kamaraj, M., Anitha, R. and Pugazhendhi, A., 2022. *In vitro* anticancer activity of silver nanoparticles phyto-fabricated by *Hylocereus undatus* peel extracts on human liver carcinoma (HepG2) cell lines. *Process Biochemistry*, 116, pp. 17-25.

Siddiqui, M.A., Alhadlaq, H.A., Ahmad, J., Al-Khedhairy, A., Musarrat, J. and Ahamed, M., 2013. Copper oxide nanoparticles induced mitochondria mediated apoptosis in human hepatocarcinoma cells. *PLOS ONE*, [e-journaal] 8(8), p. 69534. https://doi.org/10.1371/journal.pone.0069534.

Sim, S. and Wong, N.K., 2021. Nanotechnology and its use in imaging and drug delivery (review). *Biomedical Reports*, [e-journal] 14(5), pp. 1-9. https://doi.org/10.3892/br.2021.1418.

Singh, D., Jain, D., Rajpurohit, D., Jat, G., Kushwaha, H.S., Singh, A., Mohanty, S.R., Al-Sadoon, M.K., Zaman, W. and Upadhyay, S.K., 2023. Bacteria assisted green synthesis of copper oxide nanoparticles and their potential applications as antimicrobial agents and plant growth stimulants. *Frontiers in Chemistry*, [e-journal] 7(11), p. 1154128. https://doi.org/10.3389/fchem.2023.1154128.

Singh, M., Goyal, M. and Devlal., K., 2018. Size and shape effects on the band gap of semiconductor compound nanomaterials. *Journal of Taibah University for Science*, [e-journal] 12(4), pp. 470-475. https://doi.org/10.1080/16583655.2018.1473946.

Sivagami, M. and Asharani, I.V., 2022. Phyto-mediated Ni/NiO NPs and their catalytic applications – a short review. *Inorganic Chemistry Communications*, [e-journal] 145, pp. 1-15. https://doi.org/10.1016/j.inoche.2022.110054.

Soria, N.G.C., Aga, D.S. and Atilla-Gokcumen, G.E., 2019. Lipidomics reveals insights on the biological effects of copper oxide nanoparticles in a human colon carcinoma cell line. *Molecular Omics*, [e-journal] 15(1), pp. 30-38. https://doi.org/10.1039/C8MO00162F.

Tabrez, S., Khan, A.U., Mirza, A.A., Suhail, M., Jabir, N.R., Zughaibi, T.A. and Alam, M., 2022. Biosynthesis of copper oxide nanoparticles and its therapeutic efficacy against colon cancer. *Nanotechnology Reviews*, [e-journal] 11(1), pp. 1322-1331. https://doi.org/10.1515/ntrev-2022-0081.

The University of Kansas Cancer Center, 2024. *Cancer overview.* [online] Available at: <https://www.kucancercenter.org/patients-caregivers/cancer-education/cancer-overview> [Accessed 18 March 2024].

Tonder, A., Joubert, A.M. and Cromarty, A.D., 2015. Limitations of the 3-(4,5-dimethylthiazol-2-yl)-2,5-diphenyl-2H-tetrazolium bromide (MTT) assay when compared to three commonly used cell enumeration assays. *BMC Research Notes*, [e-journal] 8, p. 47. https://doi.org/10.1186/s13104-015-1000-8.

Toxicology MSDT, 2022. *3.4: Different cytotoxicity assays.* [online] Available at: <https://chem.libretexts.org/Bookshelves/Environmental_Chemistry/Toxicology_MSDT/03%3A_Principles_of_Genetic_Toxicology/3.04%3A_New_Page> [Accessed 8 March 2024].

Tran, U.P.N., Dang-Bao, T., Le, P.T.K., Huynh, U.D.H., Nguyen, T.T.H. and Le, T.M., 2022. Encapsulation of betalains extracted from red dragon fruit peels by freeze-drying using microcrystalline cellulose and dragon fruit peel pectin as wall materials. *Chemical Engineering Transactions*, [e-journal] 97(1), pp. 31-36. https://doi.org/10.3303/CET2297006.

Tulinska, J., Mikusova, M.L., Liskova, A., Busova, M., Masanova, V., Uhnakova, I., Rollerova, E., Alacova, R., Krivosikova, Z., Wsolova, L., Dusinska, M., Horvathova, M., Szabova, M., Lukan, N., Stuchlikova, M., Kuba, D., Vecera, Z., Coufalik, P., Krumal, K., Alexa, L., Vrlikova, L., Buchtova, M., Dumkova, J., Piler, P., Thon, V. and Mikuska, P., 2022. Copper oxide nanoparticles stimulate the immune response and decrease antioxidant defense in mice after six-week inhalation. *Frontiers in Immunology*, [e-journal] 13, pp. 1-12. https://doi.org/10.3389/fimmu.2022.874253.

Varughese, A., Kaur, R. and Singh, P., 2020. Green synthesis and characterization of copper oxide nanoparticles using *Psidium guajava* leaf extract. *IOP Conference Series: Materials Science and Engineering*, [e-journal] 961, p. 012011. https://doi.org/10.1088/1757-899X/961/1/012011.

Veerakumar, P., Hung, S.T., Hung, P.Q. and Priya, V.V., 2023. Synthesis of activated porous carbon from red dragon fruit peel waste for highly active catalytic reduction in toxic organic dyes. *Catalysts*, [e-journal] 13(2), p. 449. https://doi.org/10.3390/catal13020449.

Vijayaraj, R., Kumaran, N., Altaff, K., Ramadevi, S. and Rosita, A.S., 2019. In silico pharmacokinetics and molecular docking of novel bioactive compound (11-methoxy-2-methyltridecane-4-ol) for inhibiting carbohydrates hydrolyzing enzyme. *Journal of Biologically Active Products from Nature*, 9(6), pp. 445- 456.

Waris, A., Din, M., Ali, A., Ali, M., Afridi, S., Baset, A. and Khan, A.U., 2021. A comprehensive review of green synthesis of copper oxide nanoparticles and their diverse biomedical applications. *Inorganic Chemistry Communications*, [e-journal] 123, p. 108369. https://doi.org/10.1016/j.inoche.2020.108369.

WebMD, 2024. *Dragon fruit – Uses, side effects, and more.* [online] Available at: <https://www.webmd.com/vitamins/ai/ingredientmono-1580/dragon-fruit> [Accessed 30 October 2023].

Widiandani, T., Tandian, T., Zufar, B.D., Suryadi, A., Purwanto, B.T., Hardjono, S. and Siswandono, 2023. *In vitro* study of pinostrobin propionate and pinostrobin butyrate: cytotoxic activity against breast cancer cell T47D and its selectivity index. *Journal of Public Health in Africa*, [e-journal] 14(1), p. 2516. https://doi.org/10.4081%2Fjphia.2023.2516.

Wong, M.C.S., Wang, B., Lim, F.S., Teo, S.H., Huang, J.J. and Young, D., 2022. Cancer control in primary care in Asia: current challenges and future perspectives. *European Journal of Cancer Care*, [e-journal] 31(5). https://doi.org/10.1111/ecc.13580.

World Health Organization, 2024. *Global cancer burden growing, amidst mounting need for services.* [online] Available at: <https://www.who.int/news/item/01-02-2024-global-cancer-burden-growing--amidst-mounting-need-for-services> [Accessed 12 April 2024].

Wybraniec, S., Nowak-Wydra, B., Mitka, K., Kowalski, P. and Mizrahi, Y., 2007. Minor betalains in fruits of *Hylocereus* species. *Phytochemistry*, 68(1), pp. 251-259.

Yu, L., Zhu, G.X., Zhang, Z.Y., Yu, Y., Zeng, L.T., Xu, Z.D., Weng, J.L., Xia, J.Y., Li, J. and Pathak, J.L., 2023. Apoptotic bodies: Bioactive treasure left behind by the dying cells with robust diagnostic and therapeutic application potentials. *Journal of Nanobiotechnology*, [e-journal] 21, p. 218. https://doi.org/10.1186/s12951-023-01969-1.

Yugandhar, P., Vasavi, T., Devi, P.U. and Savithramma, N., 2017. Bioinspired green synthesis of copper oxide nanoparticles from *Syzygium alternifolium (Wt.)* Walp: characterization and evaluation of its synergistic antimicrobial and anticancer activity. *Applied Nanoscience*, [e-journal] 7(7), pp. 417-427. https://doi.org/10.1007/s13204-017-0584-9.